NASA CONTRACTOR REPORT

NASA CR-1604

RESEARCH ON INSTABILITIES IN ATMOSPHERIC FLOW SYSTEMS ASSOCIATED WITH CLEAR AIR TURBULENCE

by James W. Clark, Richard C. Stoeffler, and Paul G. Vogt

Prepared by
UNITED AIRCRAFT CORPORATION
East Hartford, Conn.
for

NATIONAL AERONAUTICS AND SPACE ADMINISTRATION • WASHINGTON, D. C. • JUNE 1970

NASA CR-1604

1. Clear air turbulence

RESEARCH ON INSTABILITIES IN ATMOSPHERIC FLOW SYSTEMS ASSOCIATED WITH CLEAR AIR TURBULENCE

By James W. Clark, Richard C. Stoeffler,
and Paul G. Vogt

Issued by Originator as Report H910563-9

Prepared under Contract No. NASw-1582 by
UNITED AIRCRAFT CORPORATION
East Hartford, Conn.

for

NATIONAL AERONAUTICS AND SPACE ADMINISTRATION

For sale by the Clearinghouse for Federal Scientific and Technical Information
Springfield, Virginia 22151 – CFSTI price $3.00

FOREWORD

Analytical and experimental fluid mechanics investigations were performed to investigate instabilities in atmospheric flow systems associated with clear air turbulence. This research was conducted by the United Aircraft Corporation Research Laboratories under Contract NASW-1582 with the National Aeronautics and Space Administration Headquarters, Washington, D. C., 20546. The program was under the technical direction of the Chief, Fluid Dynamics Branch, Code RRF, Office of Advanced Research and Technology.

TABLE OF CONTENTS

Research on Instabilities in Atmospheric Flow Systems Associated with Clear Air Turbulence

SUMMARY

Analytical and experimental fluid mechanics investigations were conducted to investigate instabilities in atmospheric flow systems associated with clear air turbulence.

Most of the experimental program was directed toward investigation of the stability of straight, stratified shear flows. The experiments were conducted using the UARL Open Water Channel which provides flows having wide ranges of shear, density stratification and flow curvature. The channel is 2-ft-wide by 6-in.-deep by 10-ft-long and has flexible lucite sidewalls to allow adjustment of the curvature. The flow is non-recirculating and the maximum velocity is about 1.0 ft/sec. Hot-water nozzles and tapered filter beds at the upstream end allow vertical and transverse gradients of temperature and velocity to be introduced. Observations were made using dye and hydrogen bubble traces; measurements were also made using a hot-film anemometer.

The results of the fluid mechanics investigations were then applied in an investigation of atmospheric shear flows. Aircraft and radiosonde data were used in analyses of two cases in which stratospheric clear air turbulence was associated with mountain lee waves. The analyses appear to confirm that very stable layers in the atmosphere can be destabilized by increases in shear which occur as the layers flow through lee waves.

This phenomenon can occur at all altitudes and is not limited to mountain lee wave conditions. It can be associated with shear-gravity waves that occur when there is a major inversion and strong wind shear; it can also occur when stable layers flow over the tops of large cumulonimbus clouds. Thus, the phenomenon could be responsible for an appreciable fraction of clear air turbulence encounters.

RESULTS AND CONCLUSIONS

1. The fluid mechanics experiments to investigate the stability of straight, stratified shear flows tended to confirm the theoretical stability criteria of Drazin and others. The experimental velocity and density profiles differed somewhat from the hyperbolic tangent velocity profile and exponential density profile assumed by Drazin. However, his theory and the experiments were in agreement in that, with few exceptions, (1) the flows were stable for Richardson numbers greater than 0.25 and (2) the wavelengths of the instabilities that were observed were in the range predicted by the theory to be unstable.

2. Drazin's criterion was compared with theoretical criteria for other assumed velocity and density profiles. All indicated that the flow should be stable for Richardson numbers greater than 0.25. Shorter wavelengths might be observed in some unstable shear layers. However, Drazin's theory should provide reasonably good estimates of the wavelengths that occur in atmospheric shear flows.

3. Four distinct stages were observed when the shear flows broke down. First there was a region which appeared undisturbed. Downstream of this region, waves were observed. These amplified and transitioned into vortices which then burst to form turbulence. The downstream distance at which the waves were first observed varied approximately inversely with the absolute value of the shear. As many as four or five wavelengths were often observed upstream of the first discernible vortex; thus, it is reasonable to expect that several distinct waves might be observed in the isentropes when instabilities occur in atmospheric shear layers.

4. The analyses of two mountain lee wave cases appear to confirm that very stable layers in the atmosphere can be destabilized by increases in shear which occur as the layers flow through the long-wavelength lee waves. Stable layers in the stratosphere were identified using radiosonde data. The stability of these layers in the lee-wave region was predicted by estimating the changes in shear that occurred near lee-wave peaks and troughs and applying the criterion $Ri > 0.25$ for stability. Drazin's criterion was used to estimate the unstable wavelengths that might occur in these layers. The estimated wavelengths were in good agreement with wavelengths observed in the isentropes reconstructed from aircraft and radiosonde data. Moreover, the locations of these waves and subsequent turbulence relative to the peaks and troughs of the lee waves were predicted reasonably well.

INTRODUCTION

There continues to be considerable interest in the nature and causes of clear air turbulence. This interest has been stimulated by the planned development of supersonic transport aircraft. In addition to the considerations of passenger comfort and safety, CAT is important to SST designers because of its influence on the aircraft structure, on stability and control, and on operation of the inlets and engines.

Fundamental questions remain regarding the origins of certain types of CAT. Once these origins are determined, improved criteria for predicting the occurrence of CAT can be developed and possible methods for its detection and avoidance can be evaluated.

CAT is usually associated with flow systems having wind shear and density gradients, and sometimes with curvature of the streamlines. The UARL Open Water Channel allows laboratory-scale fluid mechanics investigations of such flows to be conducted. It was constructed by United Aircraft specifically for research that would contribute to understanding of the CAT problem.

Accordingly, the principal objectives of the investigations reported herein were: (1) to gain increased understanding of the nature and causes of turbulent atmospheric phenomena, particularly clear air turbulence; (2) to develop improved criteria for predicting neutrally stable states in atmospheric flow systems; and (3) to compare the results of this research with available meteorological data and attempt correlations.

The main text of this report contains three sections --- a description of the equipment and procedures used in the fluid mechanics experiments, a discussion of an investigation of the stability of straight, stratified shear flows, and a discussion of the application of the results to atmospheric shear flows. Appendix I describes other related experiments that were conducted using the water channel. These include experiments with an oscillating plate to induce disturbances in a shear layer, experiments with standing shear-gravity waves, and experiments with the channel walls curved. Appendix II contains a summary of the results of meteorological analyses of six clear air turbulence encounters from airline, military and AFCRL-NASA experience. Appendix III contains a brief glossary of the principal meteorological terms that are used in this report.

DESCRIPTION OF EQUIPMENT AND PROCEDURES

UARL Open Water Channel

Figure 1 is a photograph of the UARL Open Water Channel and Fig. 2 is a sketch indicating its major features. This facility provides a 2-ft-wide by 6-in.-deep by 10-ft-long, non-recirculating, open channel flow. The lucite side walls extend about 2 in. above the surface of the water. They are held firmly in place by weights and the joints where the walls meet the glass-topped table which forms the channel floor are sealed. The walls can be adjusted from the straight-channel position (shown by the solid lines in Fig. 2) to any desired curved-channel position (shown by the dashed lines) with the minimum centerline radius of curvature being about 6 ft. The flow is illuminated from beneath the glass floor using fluorescent lights (visible in Fig. 1).

Tapered filter beds made from a porous foam material* are used to introduce desired vertical and transverse velocity profiles at the upstream end of the channel (Fig. 2). The foam material is bonded to porous stainless steel supporting structures which are bolted to the cover of the plenum. Several different adjustable sluices, including some that are porous, are used at the downstream end of the channel. They provide usable mean channel velocities up to about 1.0 ft/sec.

Hot-water nozzles in the plenum are used to introduce vertical and transverse temperature gradients and, hence, density stratification. Figure 2 shows schematically the nozzles used to create vertical gradients; twelve such nozzles are actually located in the plenum. Six similar nozzles (not shown) are installed with their axes vertical to create transverse temperature gradients. A filter consisting of screens and a 3-in.-thick layer of pebbles is used downstream of the hot-water nozzles to smooth the temperature profiles.

With the channel walls straight, the origin of the coordinate system used to describe points in the flow is at the juncture of the tapered filter bed, the floor of the channel, and the side wall nearest the observer (see Fig. 2); x is measured in the downstream (streamwise) direction, y is measured transversely from the wall, and z is measured vertically from the floor of the channel. With the channel walls curved, positions in the flow are described by z, by the local radius r measured from the center of curvature of the channel, and by the running coordinate s measured from the filter bed along the centerline of the channel in the downstream direction.

---

* Scott Industrial Foam, a product of the Scott Paper Company, Foam Division, 1500 East Second Street, Chester, Pennsylvania.

The central region of the channel away from the floor and side-wall boundary layers and away from the free surface is the region of primary interest. The gradients attainable in this central region vary with the local temperature of the water and with the shear-layer thickness. The approximate ranges of velocities, temperatures, and gradients in tests reported herein were:

Local Velocities:	$0.02 < V < 0.5$ ft/sec
Velocity Gradients:	$-3.5 < \partial V/\partial z < +3.5$ sec^{-1}
	$-0.3 < \partial V/\partial r < +0.6$ sec^{-1}
Local Temperatures:	$40 < T < 100$ F
Temperature Gradients:	$0 < \partial T/\partial z < +135$ deg F/ft
	$-4 < \partial T/\partial r < 0$ deg F/ft

Several experiments were also conducted with convectively unstable flows, i.e., with $\partial T/\partial z < 0$.

Use was made of the curves in Fig. 3 (derived from tabulated data in Ref. 1) for calculating the Richardson numbers* for these flow conditions. The range of Richardson number was from slightly less than 0 (for $\partial T/\partial z < 0$) to near infinity (for $\partial V/\partial z$ approaching 0).

The Reynolds numbers per unit length in the channel vary over wide ranges due to the wide ranges of both velocity and temperature. In the present investigation, the minimum value was $Re/\ell = 1200$ per ft for $V = 0.02$ ft/sec and $T = 40$ F; the maximum was $Re/\ell = 67{,}800$ per ft for $V = 0.5$ ft/sec and $T = 100$ F.

The floor of the channel slopes downward slightly toward the sluice. Thus, some provision is made for the effect on the flow of floor boundary layer growth. Nevertheless, care must be taken to assure that observations are not influenced by this boundary layer, particularly at low channel speeds. Care must also be taken to assure that the blocking effect of the sluice under low-velocity, strong-stratification conditions does not influence the observations. Under such conditions it is necessary to throughly mix the flow in the channel about every 30 to 45 minutes and then wait for the flow to settle down.

* $\overline{Ri = (-g/\rho)(\partial\rho/\partial z)}/(\partial V/\partial z)^2 = (-g/\rho)(\partial\rho/\partial T)(\partial T/\partial z)/(\partial V/\partial z)^2$; using the measured T, ρ and $\partial\rho/\partial T$ were determined from Fig. 3.

Instrumentation and Test Procedures

The principal instrumentation used with the water channel is also shown in Fig. 1.

Dye Tracing

Neutrally buoyant fluorescent dye* is used to obtain qualitative information about the nature of the flow. It is an effective method for identifying the presence of internal waves, vortices and turbulence; it can also be used to determine the wavelengths of internal waves. The dye is injected through 0.020-in.-ID stainless steel hypo tubes located immediately upstream of the tapered filter bed. The dye streamers trace out streamlines in steady flows and streaklines in unsteady flows. In the latter case, caution must be used in their interpretation (see discussion in Ref. 2).

Bubble Tracing

Measurements of the velocity profiles are made using the hydrogen bubble wire technique. A voltage is applied to a 0.001-in.-dia platinum wire extending from the channel floor through the surface of the water. Hydrogen bubbles are generated by electrolysis. The voltage may be pulsed at 10, 5, 2, or 1.0 cps to generate chains of bubbles which drift downstream with the flow. The local velocity can be determined by photographing the chains, determining the distance between chains from the photographs and dividing by the time between chains. At low speeds, only the chains closest to the wire are used to prevent errors due to rising of the bubbles. The voltage can also be applied continuously to create a sheet of bubbles for flow visualization.

Anemometry and Thermometry

A DISA Type 55D01 constant-temperature anemometer is used for measurements of velocity fluctuations. This unit is used with DISA Type 55A81 wedge-shaped hot-film probes (insulated for use in conducting media), a Type 55D30 digital voltmeter, and a Type 55D35 rms unit. The probes are calibrated using bubble-trace measurements to obtain velocity-voltage correlations. The highest frequencies of interest in the water channel are less than 100 cps while the frequency response of the probe and anemometer is approximately linear up to 2,000 cps. The probe is mounted such that it can be traversed in the vertical and transverse directions at any downstream location in the channel.

---

* Uranine concentrate powder in water; concentrate available from Sagamore Color & Chemical Co., 82 Braintree Street, Alston Sta., Boston, Mass.

Some measurements of temperature were made using a hot-film probe as a resistance thermometer. However, all of the temperature measurements reported herein were made using a standard submersible mercury-filled thermometer.

INVESTIGATION OF THE STABILITY OF STRAIGHT, STRATIFIED SHEAR FLOWS

Introduction

The primary purpose of the fluid mechanics program was to experimentally examine the stability characteristics of straight, stratified shear flows. The end objective was to apply the results to thin, initially stable shear flows occurring in the atmosphere. Accordingly, the program was directed toward three areas: (1) answering certain questions concerning the conditions under which such flows become unstable, (2) determining the characteristics of the flow during the initial phases of breakdown, and (3) verifying one or more of the existing theoretical criteria for subsequent use in studying atmospheric shear flows.

A great many investigators have performed theoretical studies to develop criteria for instabilities in straight, inviscid, stratified shear flows. A thorough and up-to-date summary of these theoretical studies appears in Ref. 3. Of the references cited therein, the most pertinent to the present investigation are by Drazin (Ref. 4), Drazin and Howard (Ref. 5), and Miles and Howard (Ref. 6). Two-dimensional flow is assumed and analytic functions are used to represent the vertical profiles of velocity and density. It is also assumed that the change in density across the shear layer is small. With some exceptions (Ref. 3), the flow is assumed to be unaffected by confining walls or a free surface.

The most fundamental and frequently encountered flow consists of two uniform streams which have different velocities and which are separated by an intermediate shear layer as shown in the sketch. Velocity profiles of this type are readily created in the UARL Open Water Channel by shaping the foam material in the filter bed as shown. The "hyperbolic tangent" velocity profile used by Drazin (Ref. 4) and others most closely approximates the profiles in the channel:

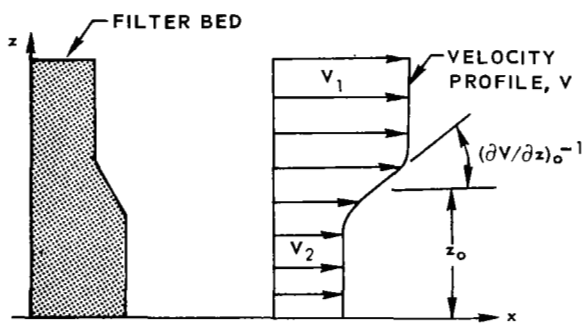

$$V = V_o + \frac{\Delta V}{2} \cdot \tanh\left(\frac{z - z_o}{d}\right) \qquad (1)$$

In this equation, V is the local velocity at height z above the channel floor; $V_o = (V_1 + V_2)/2$ is the velocity at the center of the shear layer at height z_o; $\Delta V = (V_1 - V_2)$; and $d = (\Delta V)/2(\partial V/\partial z)_o$. The latter parameter is a scale length and is approximately half the thickness of the shear layer. Drazin also uses an exponential variation of density with height:

$$\rho/\rho_0 = e^{-\beta\left(\frac{z-z_0}{d}\right)} = e^{-\frac{Ri \cdot d \cdot (\partial V/\partial z)_0^2}{g}\left(\frac{z-z_0}{d}\right)} \tag{2}$$

where Ri is the Richardson number and g is the gravitational constant. Since the change in density across the shear layer is small, a good approximation to Eq. (2) is

$$\rho/\rho_0 = 1 - \frac{Ri \cdot d \cdot (\partial V/\partial z)_0^2}{g}\left(\frac{z-z_0}{d}\right) \tag{3}$$

Drazin derives a criterion for stability in Ref. 4 by introducing a perturbation stream function

$$\psi' = \phi(z) \cdot e^{i\alpha(x-ct)} \tag{4}$$

into the equations governing the motion of the fluid. Here, α is the wave number, $\alpha = 2\pi/\lambda$, and c is the complex wave velocity, $c = c_r + i\, c_i$. The equations of motion then yield a single stability equation. Making use of the fact that the perturbations neither amplify nor decay when $c_i = 0$, Drazin solves for the following equation for neutral stability on the αd - Ri plane:

$$\alpha d = \sqrt{\frac{1}{2} \pm \sqrt{\frac{1}{4} - Ri}} \tag{5}$$

The sketch at the right shows this boundary and the adjacent stable and unstable regions. The criterion indicates that the flow would be stable for disturbances of all dimensionless wavenumbers, αd, for $Ri > 0.25$. For $Ri < 0.25$, it would be unstable for dimensionless wavenumbers which lie inside the boundary.

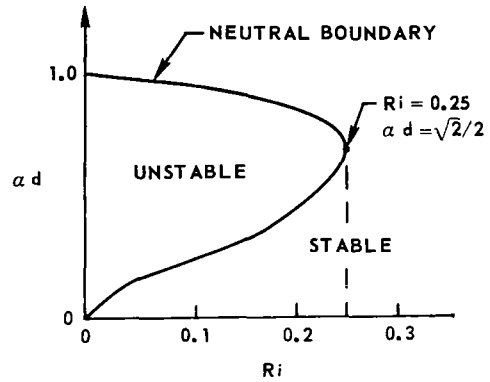

The preceding theoretical considerations formed the basis for planning the experiments. Several important features needed to be verified and/or investigated experimentally to provide information for the analyses of atmospheric shear flows. In particular, it was desired to verify the discrete wave-like nature of the initial disturbance and to obtain a method for estimating the wavelengths that occur. Next, it was desired to observe the stages through which initial disturbances proceed to breakdown into turbulence; the greater the number of wavelengths that occur upstream of the turbulence, the greater the probability of detecting small waves on isentropes upstream of turbulent regions in the atmosphere. It was also desired to determine whether or not Drazin's criterion, or a similar criterion, could be broadly applied to shear flows without detailed consideration of every small "kink" in the velocity and density profiles. Finally, it was hoped that the results would provide further evidence that $Ri = 0.25$ should be used as a critical Richardson number in atmospheric analyses since there is still discussion of this point among theoreticians (e.g., Refs. 7 and 8).

Summary of Experimental Results

Velocity, Temperature, and Density Profiles

Velocity, temperature, and density profiles for three typical flow conditions are shown in Fig. 4. These data are for three different Richardson numbers: $Ri = 0.054$ (Fig. 4(a)), $Ri = 0.141$ (Fig. 4(b)), and $Ri = 0.575$ (Fig. 4(c)). The velocity and temperature measurements were made within 5 to 10 in. downstream of the filter bed. As noted previously, use was made of the curve in Fig. 3(a) for calculating the density profiles from the temperature profiles. The corresponding velocity and density profiles in Drazin's theory (Eqs. (1) and (3)) are shown by the dashed lines.

These particular velocity profiles were selected because they show the typical differences that existed between water channel velocity profiles and the corresponding ideal hyperbolic tangent profiles of Drazin. Over the central portion of the shear layer the similarity was good. The differences usually appeared near the edges of the shear layer (particularly near the low-velocity edge). Further comments on the small influence which these differences appear to have on the stability of the flow are included later in the report.

The three velocity profiles all show positive shear, i.e., $\partial V/\partial z > 0$. Many tests were run with inverted filter beds (foam material thicker above the shear region than below it) so as to create negative shear, i.e., $\partial V/\partial z < 0$. The only effect of the change in sign of the shear was to reverse the circulation of the vortices which formed in the breakdown region. From an operational standpoint, however, it was more satisfactory to have the higher velocity stream on top so as to minimize the effects on the velocity profile when changes were made in the flow through the hot-water nozzles.

The significant feature to note about the temperature profiles (Fig. 4) is that the gradients were fairly uniform or increased steadily from near the floor to near the surface. That is, there were no steep local gradients analogous to the steep velocity gradients in the shear layer.

The experimental and theoretical density profiles (Fig. 4) were similar over only a portion of the shear layer. The smaller the density gradient, the larger the distance over which the profiles were similar (compare Figs. 4(a) and (c)). The primary reason for this is that $\partial\rho/\partial T$ is a strong function of water temperature, particularly at low temperatures. As shown in Fig. 3(b), water has a maximum density ($\partial\rho/\partial T = 0$) at about 39.2 F; this is the reason why the density is essentially constant ($\partial\rho/\partial z$ approaches zero) below the shear layer in all three profiles. The control of density could be improved if provision were made to preheat all of the incoming water from its temperature in the main to perhaps 60 or 70 deg.

Characteristics of Breakdown of Flow

Flow Visualization Using Dye Traces

Figure 5 illustrates the stages observed as the flow in the shear layer breaks down. There are four very distinct and repeatable stages which occur; dye traces illustrating the phenomenon are shown in the sketch and in the photographs. The photographs were taken through the lucite side wall (Fig. 2); the flow is from left to right. The scale appearing in the photographs was immersed in the flow close to the dye traces.

In Fig. 5(a), the flow appears undisturbed. Neither the dye traces nor the hydrogen bubble traces show visual evidence of any perturbation.

In Fig. 5(b), which is 8 in. further downstream, the center dye trace indicates the presence of a wave amplifying as it progresses downstream. The wave has a wavelength of about $\lambda = 5.5$ in. and an amplitude (half the distance from trough to peak) of about $a = 0.1$ in. at this point. By placing dye probes at several transverse locations it was verified that the flow was approximately two-dimensional, i.e., the wave extended across the channel.

In Fig. 5(c), which is another 19 in. downstream, the waves have rolled up into vortices. The circulation of the vortices has the same sense as the vorticity introduced by the shear --- the shear is negative in this flow condition, and all of the vortices rotated counterclockwise. These vortices grew slightly in size as they drifted downstream. Their downstream drift velocity was checked and found to be approximately V_o, the velocity upstream at the center of the shear layer. The flow was also determined to be two-dimensional at this stage. (The small kinks in the dye streamer in the lower left center of the photograph are not related to the flow pattern. These occur occasionally when a drop or two of dye that is slightly more dense than the rest comes through the probe.)

In Fig. 5(d), which is another 28 in. downstream --- 66 in. downstream of the filter bed --- the vortices have "burst" and the flow appears turbulent. The fluid motions were three-dimensional at this stage.

Experiments were conducted in which dye was injected into the vortices as they drifted past a dye probe fixed in the channel at $x = 40$ in. Attempts were also made to obtain instantaneous velocity profiles by triggering a bubble wire as the vortices drifted past. Both the dye and the bubbles indicated the presence of strong circulation. Further measurements should be made to thoroughly investigate the vortex velocity profiles immediately upstream of the point of bursting.

These observations are in agreement with the theoretical analysis of Michalke (Ref. 9). He calculated lines of constant vorticity and streaklines for a hyperbolic tangent velocity profile for $Ri = 0$. His results show concentrations of vorticity which superimpose a rotational motion on the basic flow. The observations are also similar to those of Freymuth (Ref. 10). In an experiment with a free air jet, he excited disturbances in the high-shear region using acoustic waves. His smoke traces show a similar development pattern.

Anemometer Measurements

Sections of anemometer traces for each of the four stages in the breakdown are shown in Fig. 6. The approximate values of the peak velocity fluctuations at the predominant wavelengths were obtained from the traces and are shown in Fig. 7.

Figure 6(b) through (d) shows substantial changes in the shape of the probe voltage output as the flow transitions from waves to initial turbulence. As indicated in Fig. 7(a), (b), and (c), there was a strong component at $\lambda = 6$ in., the approximate wavelength of the initial waves. This component increased from $\Delta V(\lambda)/V_o \times 100 = 1$ percent at $x = 20$ in. to about 11.3 percent in the turbulent region. In the vortex region (Fig. 7(b)), a component appeared at $\lambda/2$; additional components appeared in the turbulent region, some around $\lambda/4$. Thus, there appears to be a cascading of energy from the wavelength of the initial perturbation to the higher harmonics as the breakdown progresses.

Comparison of Results with Theoretical Stability Criteria

Comparison with Drazin's Criterion

Figure 8 is a summary of the results and a comparison with Drazin's theoretical criterion. For each flow condition, the Richardson number was calculated using the slopes $(\partial V/\partial z)_o$ and $\partial T/\partial z$ from the measured profiles. The scale length, d, was calculated using the slope $(\partial V/\partial z)_o$ and the velocity difference ΔV from the velocity profile; ΔV was based on the maximum and minimum velocities in the vicinity of the edges of the shear layer (Fig. 4). The wavenumber, $\alpha = 2\pi/\lambda$, was calculated using wavelengths determined from photographs of the dye traces. Thus, each flow condition at which waves were observed is identified by a point on the plot of αd vs Ri.

The different symbols in Fig. 8 denote different flow characteristics that were observed. The open circle symbol denotes conditions at which only waves were observed; that is, the waves extended the entire length of the channel without transitioning to vortices. The wavelengths of these waves ranged from about 3 to 6 in. The flags shown on the open circle symbols in the symbol block indicate the nature of the disturbances observed --- for example, small-amplitude waves (such as those in Fig. 5(b)) which persisted, waves which seemed to grow in amplitude to a certain point and then not grow further as they progressed downstream, and waves which appeared in the flow only intermittently. The half-solid symbol denotes flow conditions at which the waves transitioned to vortices but did not transition to turbulence before reaching the downstream end of the channel. The full-solid symbol denotes flow conditions at which the full sequence of events occurred --- waves, vortices and turbulence. The crosses indicate conditions at which no waves of the

type associated with instability occurred. At some conditions (indicated by (SW)), standing, long-wavelength (12 to 24 in.), shear-gravity waves occurred. These shear-gravity waves were investigated in some detail and are discussed in Appendix I.

Examination of Fig. 8 indicates that most of the observations are in reasonably good agreement with Drazin's boundary. All cases at which full transition was observed fall in the unstable region. One case in which suppressed waves and vortices were observed falls above the boundary (Ri = 0.052, $\alpha d = 1.15$); two cases of intermittent waves and one of steady waves also fall above the boundary and at Ri < 0.25. These four cases could be attributed to differences between the experimental velocity profile and Drazin's hyperbolic tangent profile (this point is discussed later). The intermittent waves indicated at Ri = 0.42 and the steady waves at Ri = 0.38 are thus the only unexplainable points. There are no indications of errors in calculating the Richardson numbers. It is possible (but not likely) that the channel conditions changed after the bubble trace photographs were taken and the temperature measurements were made.

The shear, $(\partial V/\partial z)_o$, appears to be the primary factor in determining whether or not the initial waves transition to vortices and turbulence within the 120-in. length of the channel. Figure 9 shows the locations at which waves, vortices, and turbulence were first observed in each test. These data are for values of Ri between 0 and 0.25 (no trend with Ri could be seen in the data). The trend indicates that the distance downstream at which waves were first discernible varied inversely with the absolute value of the shear (Fig. 9(a)). This trend can be understood by examining the growth of Helmholtz waves which form between two adjacent (d = 0) uniform streams without stratification. The ratio of the amplitude of a wave at a distance x downstream to its amplitude at x = 0 (derived from the definition of Helmholtz instability in Ref. 11) is given by

$$\frac{a(x)}{a(0)} = e^{\pi \cdot x \cdot |\Delta V| \cdot / V_0 \cdot \lambda} \qquad (6)$$

Equation (6) may be written as

$$\frac{a(x)}{a(o)} = e^{\pi \cdot x \cdot |(\partial V/\partial z)_o| \cdot 2d/V_o \cdot \lambda} \tag{7}$$

If it is assumed that a(o) is independent of the flow condition and that some small amplitude is necessary before a wave can be seen, then the value of a(x)/a(o) at which waves will be seen would be a constant. From Eq. (7), with d, V_o, and λ constant,

$$x = \frac{\text{CONSTANT}}{|(\partial V/\partial z)_o|} \tag{8}$$

which is the trend shown in Fig. 9(a).

Curves have been drawn through the data in Figs. 9(b) and (c) to illustrate the general trends in the locations of the first vortices and turbulence that were observed. On the basis of these data, it is fairly certain that most of the open and half-solid symbols in Fig. 8 would have been solid symbols (indicating complete transition to turbulence) if the water channel had been longer. The flow conditions at which intermittent waves were observed are exceptions.

The number of wavelengths which were observed between the first discernible wave and the turbulence varied with the shear. Four of five distinct wavelengths often occurred upstream of the first vortex.

Theoretical Criteria for Other Velocity and Density Profiles

Theoretical criteria for profiles other than Drazin's are discussed in Refs. 3 and 12. All of these criteria indicate flow stability for Ri > 0.25. The neutral boundaries on the αd vs Ri plot differ somewhat, although for velocity profiles reasonably similar to those of the experiments, none predict instabilities having αd greater than about 2. An example (from Ref. 12) is shown in Fig. 10. Hazel's velocity profiles (Fig. 10(a)) in this example are nearly sinusoidal; they resemble the experimental profile shown in Fig. 4(c). His density profiles also differ from Drazin's, although most of the difference is outside of the shear layer. A comparison of Drazin's and Hazel's criteria is shown in Fig. 10(b). They both predict stability for Ri > 0.25. In addition, Hazel's criterion indicates that somewhat shorter wavelengths (larger values of αd) might be observed in unstable flows having velocity profiles which differ significantly from the hyperbolic tangent profile.

Concluding Remarks

The primary results of the fluid mechanics experiments which are applied to atmospheric shear flows in the following section are summarized here.

First, the experiments indicate the general applicability of theoretical criteria such as those of Drazin, Hazel, Howard, Miles, and others which are based on the stability of the governing equations of motion to small perturbation waves. In particular, they tend to confirm Drazin's criterion even though the experimental velocity and density profiles differed somewhat from his assumed profiles. The theoretical criteria of Hazel, which are for different velocity and density profiles, are different from Drazin's criterion only in that one might expect to observe somewhat shorter wavelengths in unstable shear layers. Drazin's boundary, however, would provide reasonably good estimates of the wavelengths that might occur. The experiments and all of the theories indicate that 0.25 should be used as the critical Richardson number. Finally, as many as four or five wavelengths were often observed upstream of the first discernible vortex; thus, it is reasonable to expect that several distinct waves might be observed in the isentropes when instabilities occur in atmospheric shear layers.

APPLICATION TO ATMOSPHERIC SHEAR FLOWS

Introduction

It is well known that stratified shear layers analogous to those investigated in the water channel experiments are common in both the ocean and the atmosphere. For example, in recent papers by Woods (Refs. 13 through 16), the results of in situ studies of flows within the ocean's thermocline were reported. Woods made detailed measurements of velocity and temperature profiles in the thermocline. He found many distinct stable layers up to about 10 cm in thickness in which the shear and/or the temperature gradient were approximately constant. By releasing neutrally buoyant dye in certain of these layers, he was able to observe the flow characteristics. In some cases, the layers underwent long-wavelength undulating motions --- wavelengths up to about 30 meters and amplitudes up to about 1.0 meter --- and the flow within the layers appeared to transition to turbulence. Woods' dye trace photographs of these transition regions are very similar to dye trace photographs of shear-layer breakdowns observed in the water channel (e.g., compare Fig. 14 of Ref. 13 with Fig. 5 of the present report).

Woods pointed out that these breakdowns within initially stable layers were a direct result of the long-wavelength undulating motions. He used an equation he obtained from a theoretical development in Phillips (Ref. 17) to show that, for certain layer and long-wave conditions, the change in shear which occurs within the layer as the flow approaches a peak or trough of the long wave can cause the local Richardson number to decrease below Ri = 0.25. Hence, the flow becomes unstable. This mechanism will be explained in more detail subsequently. The reasoning Woods applied appears to support his observations quite well.

Woods and other investigators have recognized that similar flow conditions could exist in the atmosphere. Phillips (Ref. 17) and others have discussed the fundamental mechanism by which long-wavelength undulating motions can lead to the instability of initially stable shear layers. Ludlam (Ref. 18) related certain types of billow clouds and clear air turbulence to instabilities in shear layers; he also noted that such instabilities tend to occur at high altitudes downstream of mountains. Other investigators have made contributions which are indirectly related. One of these is Mitchell (Ref. 19); in WU-2 flights in the stratosphere, he observed a correlation between clear air turbulence and layers having strong temperature stratification. Another is Spillane (Ref. 20) who also noted a correlation between stratospheric CAT over Woomera in the Australian desert and sharp, stable "kinks" in the temperature profile. A third is Hardy (Ref. 21) who has obtained radar returns from trains of 1.0- to 3- or 4-nmi waves with associated smaller-scale turbulence in regions where aircraft were reporting CAT. Hardy has also associated these waves with the breakdown of shear layers.

The possible connection between Woods' observations and clear air turbulence in the atmosphere was brought to the attention of the present authors by Professor R. W. Stewart (Ref. 22). Subsequently, using the experimental results and the theoretical criteria described in the preceding section of this report as a basis, analyses were conducted of several clear air turbulence cases in which the mechanism observed by Woods might have occurred. Two of these cases are described in this section of the report.

Fundamentals of the Flow Condition

A schematic of the flow condition is shown in Fig. 11(a). At the left are shown upstream wind and temperature profiles with a stable shear layer having a thickness 2d. Within this layer, the mean wind is V_o and the mean temperature is T_o; the shear is $(\partial V/\partial z)_o$ and the environmental lapse rate is $\partial T/\partial z$.

At the right in Fig. 11(a) is shown a portion of a long-wavelength wave having an amplitude a (which might be 2,000 or 3,000 ft) and a wavelength λ_{LW} (which might be 10 or 20 nmi). It is assumed in this analysis that the thickness of the shear layer, the mean temperature and the lapse rate all remain constant as the flow within the shear layer experiences the undulating motion (2d, T_o, and $\partial T/\partial z$ are constant). From Phillips (Ref. 17), the following equation for the increase in shear that occurs at the peak (see Fig. 11(a)) can be derived:

$$\Delta(\partial V/\partial z) = \left[N_M^2 - n^2\right](a/V_o) \tag{9}$$

For flows in the atmosphere instead of the ocean,

$$N_M = \text{Brunt - Väisälä frequency} = \sqrt{\frac{g}{T_o}\left[(\partial T/\partial z) - (\partial T/\partial z)_{ad}\right]}$$

$$n = \text{wave frequency} = 2\pi V_o/\lambda_{LW}$$

$$(\partial T/\partial z)_{ad} = \text{adiabatic lapse rate, } -2.98 \times 10^{-3} \text{ deg C/ft*}$$

This increase in shear is added to the initial shear. An expression for the minimum Richardson number (which occurs locally at the peak in the example given but would occur at the trough if the initial shear were negative) is

---

* Note use of minus sign to denote temperature decreasing with increasing altitude.

$$Ri_{MIN} = \frac{N_M^2}{\left[|(\partial V/\partial z)_o| + \Delta(\partial V/\partial z)\right]^2} \tag{10}$$

Since $N^2_m \gg n^2$ under all conditions of interest (this is only untrue for weakly stable lapse rates, i.e., when $\partial T/\partial z \approx (\partial T/\partial z)_{ad}$), the expression can be further simplified to

$$Ri_{MIN} \approx \frac{N_M^2}{\left[|(\partial V/\partial z)_o| + N_M^2(a/V_o)\right]^2} \tag{11}$$

From Eq. (11) it is evident that low values of Ri_{MIN} are associated with large initial shears, $(\partial V/\partial z)_o$; with large long-wave amplitudes, a; and with low winds, V_o. The latter two parameters are not independent, however, since large amplitude waves do not usually occur under low-wind conditions. The effect of the environmental lapse rate, $\partial T/\partial z$, on Ri_{MIN} is not evident from Eq. (11) but can be seen in Fig. 11(b). This figure is based on typical conditions under which mountain lee waves are observed in the lower stratosphere (see, for example, details of the two lee-wave cases that are described later in this section of the report). Curves are shown for two shears --- a small shear (1 kt/1,000 ft) and a moderately large shear (12 kts/1,000 ft). The curves show the somewhat surprising result that the greater the initial stability (i.e., the greater $\partial T/\partial z$), the lower Ri_{MIN} will be. They also show that slightly stable layers are not likely to become unstable unless the initial shear is large. Thus, it is primarily the most stable layers appearing in the temperature profile that are of interest.

Wavelengths of Instabilities that Might Occur

The results of the fluid mechanics experiments discussed previously tend to confirm the theoretical criterion of Drazin (Ref. 4). The theoretical critical Richardson number of 0.25 and Drazin's theoretical variation of dimensionless wavenumber with Richardson number for neutral stability (see Fig. 8) were therefore used to predict the wavelengths that might occur when an instability occurs in an atmospheric shear flow. These predictions are shown in Fig. 12.

In Fig. 12, the ranges of unstable wavelengths (λ in nmi) are shown as functions of the shear-layer thickness (2d in ft) for local values of Ri between 0.25 and 0. Considering first Ri = 0.25 (Fig. 12(a)), only one wavelength is unstable at each value of 2d --- $\lambda = (2\pi/\sqrt{2}) \cdot 2d$. This is the wavelength

corresponding to $\alpha d = \sqrt{2}/2$, the only point at which Drazin's boundary reaches as far out as Ri = 0.25 in Fig. 8. For smaller values of Ri --- Figs. 12(b), (c) and (d) --- there are increasingly wider ranges of unstable wavelengths.

One can argue several different ways to reach the conclusion that, when an instability occurs, the wavelength that will be observed will be $\lambda = (2\pi/\sqrt{2}) \cdot 2d$. This wavelength (or very nearly equal wavelengths in other theories) is often said to be "the most likely" or "the most unstable" wavelength based on its theoretical growth rate. However, another viewpoint is that if the Richardson number at the peak of the long-wavelength wave is less than 0.25, then the flow in the shear layer must have experienced Ri = 0.25 on the way up to the peak. Since instability would occur at Ri = 0.25, the wavelength that would be seen would therefore correspond to that for Ri = 0.25, or $\lambda = (2\pi/\sqrt{2}) \cdot 2d$.

Other factors enter into consideration when determining the expected wavelengths. For example, the usual radiosonde profile is based on data only at mandatory reporting altitudes and altitudes at which significant changes take place. Perhaps additional data points would lead to choice of other shear-layer thicknesses. Also, as the sounding balloon rises to stratospheric altitudes, inaccuracies may result because it has drifted downstream and thus does not provide a true vertical profile at the observing station. Furthermore, the velocity and density distributions in the shear layer will not be exactly those assumed by Drazin. This is likely to lead to slightly different wavelengths, although the effects of variations in the profiles have been shown to be small (see previous discussion and Fig. 10).

Thus, all that can be said is that $\lambda = (2\pi/\sqrt{2}) \cdot 2d$ should provide a reasonable estimate of the unstable wavelengths that can be expected. As shown in Fig. 12, the expected wavelength for 2d = 1,000 ft is 0.7 nmi, and for 2d = 5,000 ft it is 3.6 nmi. Nicholls (Ref. 23), in analyses of his stratospheric lee-wave data over the southwestern U.S., has consistently found stable layers from 1,000 to 5,000 ft thick with internal waves (as determined from reconstructed isentropes) having wavelengths from 1.0 to 3 nmi. These observations are in very good agreement with the predictions in Fig. 12(a).

Analyses of Lee Wave Cases

California Lee Wave Case

During the winters of 1966-1967 and 1968-1969, Canberra and RB-57F flights were made over the southwestern U.S. to study stratospheric waves and CAT under mountain lee wave conditions. Certain of the aircraft and radiosonde data were transmitted to the authors by Mr. J. M. Nicholls of the British Meteorological Office who participated in these flights (Refs. 23 and 24). All of the 1966-1967 data will be published in Ref. 25.

As noted previously, by reconstructing isentropes* using radiosonde and aircraft temperature measurements, Nicholls has found stable layers and small-wavelength internal waves in many of his cases. He found these stable layers flowed through standing lee waves which had wavelengths of 6 to 16 nmi and amplitudes (half the height from peak to trough) up to 3,500 ft. The stable layers ranged in thickness from 1,000 to 5,000 ft. The internal waves had wavelengths of 1 to 3 nmi and amplitudes up to 1,500 ft. The CAT usually appeared in the troughs of the long-wavelength features downstream of the small internal waves. The number of small waves that occurred upstream of the turbulence varied; four were noted often (Ref. 24).

Figure 13, which is based on a similar figure provided by Nicholls, shows an isentrope for a flight near the San Bernardino Mountains in Southern California at about 37,000 ft on February 3, 1967. The wind is from left to right (west to east) in this figure. According to Nicholls (Ref. 24):

> "The major peaks of the isentrope were fixed relative to the mountains, and the inferred stationarity implies the long-wavelength features are representative of mountain-wave airflow. The position of the wavelets and turbulence on the run and its reciprocal (which was on a parallel track 10 nmi to the north) are clearly marked. The wind direction was about 50 deg to the flight track and, assuming all peak and trough axes are normal to the wind direction, the true wavelengths would be just above one-half of those shown in the diagram, i.e., about 0.9 nmi for the wavelets, with a mountain wave separation of about 15 nmi. The turbulence and wavelets appeared to be present in the stable air brought down from 41,000 ft by the mountain wave."

Wind and temperature profiles for this case are shown in Fig. 14. Two very stable layers are evident at altitudes near the 37,000-ft flight level (Fig. 14(b)). The upper layer is approximately 2,600 ft thick; the Richardson number was calculated to be $Ri_o = 77.6$. The expected wavelength from an instability in this layer is $\lambda_{E(1)} = (2\pi/\sqrt{2}) \cdot 2{,}600 = 11{,}560$ ft, or 1.9 nmi. The shear is positive which would suggest that if an instability were to occur it would be near a peak of

---

* From the radiosonde data, the profile of potential temperature was determined. Aircraft measurements of temperature along the flight path were converted to potential temperature. It was assumed that the potential temperature profile was unchanged by the wave. Then, the height of any specific isentrope relative to the aircraft was determined from the profile and the potential temperature at the aircraft. Actual aircraft altitude was then used to locate the isentrope relative to sea level.

a lee wave instead of near a trough. The lower layer is approximately 900 ft thick and the corresponding expected wavelength is $\lambda_{E(2)} = 0.7$ nmi. The Richardson number for this layer is $Ri_o = 8.7$. The shear is negative, so that an instability would be expected near a trough of a lee wave. These and other characteristics of the expected waves that will be discussed subsequently are summarized under "California Case" in Table I.

If it is assumed that the radiosonde data are representative of undisturbed conditions upstream of the mountain waves, then the minimum Richardson number that would be expected to occur in the stable layer is given by Eq. (10). This assumes that the shear determined from the radiosonde profile, $(\partial V/\partial z)_o$, is changed by an amount $\Delta(\partial V/\partial z)$ determined from Eq. (9) using the observed long-wavelength characteristics from Fig. 13 and the characteristics of the individual layers from Fig. 14. Thus, for these calculations the following were used with the appropriate dimensional units:

Layer	λ_{LW}, nmi	a, ft	T_o, deg C	$\partial T/\partial z$, deg C/1,000 ft	V_o, kts	$(\partial V/\partial z)_o$, kts/1,000 ft
1	17	3,500	-59.2	2.9	34	+2.0
2	17	3,500	-58.9	2.6	55	-5.8

The results of these calculations are shown in Table I under "Ri_{MIN} --- based on $\Delta(\partial V/\partial z)$." It will be noted that the shear decreased the Richardson numbers greatly. In layer 1, Ri decreased from 77.6 to 0.28; in layer 2, it decreased from 8.7 to 0.52. Strict application of the criterion $Ri_{MIN} < 0.25$ for instability leads one to conclude that an instability would not occur and, hence, small waves would be unlikely. However, the calculated value for one of the two layers (layer 1) is very close to the critical value. A slight increase in shear --- about 6 percent --- above that estimated using Eq. (9) would result in $Ri < 0.25$, in which case waves would be likely.

To obtain the minimum value of Ri_{MIN} that can reasonably be derived from a given set of temperature and velocity profiles, $2\Delta(\partial V/\partial z)$ can be used in Eq. (10) instead of $\Delta(\partial V/\partial z)$. The reason for this is that, at least in theory, the difference in shear between a peak and a trough is $2\Delta(\partial V/\partial z)$. In the unlikely circumstance that the radiosonde was not taken upstream in undisturbed air but instead passed upward through a trough (in the case of positive $(\partial V/\partial z)_o$), then the change in shear would be $2\Delta(\partial V/\partial z)$. It is fairly certain that the radiosondes in this case and the case to be described subsequently were not in undisturbed air, although there is no evidence that they were taken precisely through troughs or peaks.

The values of Ri_{MIN} based on $2\Delta(\partial V/\partial z)$ are also shown in Table I. For both layers, Ri_{MIN} was much less than 0.25. Thus, under the specified conditions, both of the layers would be classified as unstable and waves would be expected.

The principal results of this analysis can be seen upon examination of Table I and Fig. 13. The calculations indicate that at least one wavelength should appear ($\lambda_{E(1)}$ = 1.9 nmi) and that a second might appear ($\lambda_{E(2)}$ = 0.7 nmi). The isentropes in Fig. 13 show several sets of small waves having wavelengths of about 0.9, 0.95, 1.2, 1.3, and 1.5 nmi; these wavelengths are quite close to the expected values. Moreover, $\lambda_{E(1)}$ = 1.9 nmi was expected near a peak and the longest wave observed, λ_0 = 1.5 nmi, occurred downstream of a peak; similarly, $\lambda_{E(1)}$ = 0.7 was expected in a trough and waves having λ_0 = 0.9, 0.95, 1.2, and 1.3 nmi were all observed in a trough. Finally, it should be mentioned that the potential temperature for layer 2 was calculated to be θ = 334 K; this is very close to θ = 333 K, which is the isentrope shown in Fig. 13. The small waves in this specific isentrope are evidence that layer 2 did in fact become unstable.

Nicholls has indicated that when stable layers such as those shown in the temperature profile in Fig. 14(b) occur, they are clearly identifiable in widely dispersed upstream soundings (Ref. 23). He has observed the same detailed temperature structure in as many as five soundings spread out over several hundred miles. The detailed velocity structures show the same magnitude shears but with more-or-less random variations in the altitudes at which they occur.

Before leaving this case, it should be mentioned that Eq. (9) is theoretically valid only for a single isolated stable layer subjected to an undulating motion. There is some question regarding its use when two or more layers are close together as in the present case (Fig. 14). Calculations were made in which layers 1 and 2 and the intermediate layer were "lumped". The average values of temperature, lapse rate and wind velocity (but not initial shear) for the "lumped" layer were used to evaluate Ri_{MIN} within each individual layer. The calculated values of Ri_{MIN} differed somewhat from those shown in Table I; however, the conclusions regarding the likelihood of waves occurring were not changed at all. Similar results were obtained with the case to be discussed next in which many more layers were present. Thus, it does not appear to make much difference whether the layers are treated as isolated layers or as a single "lumped" layer when assessing stability.

There is a possibility that once small waves occur, some interaction will take place between waves in adjacent layers resulting in modification of the observed wavelengths and amplitudes. Resonant coupling between waves in highly stable layers and resulting amplitude modulation has been investigated in the ocean (Ref. 26). The existence of such effects in atmospheric flows of the type considered in this report should also be investigated.

Colorado Lee Wave Case

A similar analysis was conducted for a case near Boulder, Colorado on February 15, 1968. This case was well documented by Dr. Douglas K. Lilly of the National Center for Atmospheric Research. A description of the case, which was prepared before it was realized that the phenomenon under consideration in the present investigation was involved, was given in Ref. 27. Additional data for use in the present analysis were obtained from Dr. Lilly.

The isentropes are shown in Fig. 15. Three aircraft participated in the experiment, and the three groups of isentropes indicate the approximate ranges of altitudes in which flights were made. The flight between 50,000 and 60,000 ft, which is the altitude range of primary interest due to the small waves and turbulence that were encountered, was made by the U.S.A.F. HICAT U-2 airplane.

The wind was from west to east (left to right) in Fig. 15. Lee waves are evident at all altitudes. In the 50,000-to-60,000-ft range, these waves had average wavelengths of about 18 nmi and amplitudes (half the height from peak to trough) up to about 3,000 ft. Two radiosondes were used in this analysis. One was launched at Granby (Fig. 16(a) and (b)) which is upstream in the mountains approximately 35 nmi west-northwest of the Marshall radar. The second was launched at Denver (Fig. 16(c) and (d)) which is downstream approximately 22 nmi southwest of the Marshall radar.

Six highly stable layers were identified in each of the two radiosonde temperature profiles in Fig. 16. There is considerable similarity between the two temperature profiles which were about 55 nmi apart. The corresponding stable layers in the profiles are as follows (the Granby layer is given first): 1 and 8, 2 and 9, 3 and 10, 5 and 11, and 6 and 12. Only layers 4 and 7 do not appear in both profiles.

The wavelengths that would be expected if instabilities were to occur were computed using $\lambda_E = (2\pi/\sqrt{2}) \cdot 2d$ and are shown in Figs. 16(b) and (d). Layers which were subsequently found to be stable when $2\Delta(\partial V/\partial z)$ was used in computing Ri_{MIN} are denoted by an asterisk.

The characteristics of the expected and observed waves are summarized in Table I under "Colorado Case." The layers have been grouped according to their altitudes. The first seven have mean altitudes between 57,715 and 67,195 ft and are associated with the upper group of isentropes in Fig. 15; the remaining five have mean altitudes between 37,967 and 47,112 ft and are associated with the middle group of isentropes.

The principal results of this analysis can be seen upon examination of Table I and Fig. 15. Consider the upper group of isentropes first. The calculations indicate that at least two wavelengths should appear ($\lambda_{E(2)} = 2.4$ nmi and $\lambda_{E(7)} = 0.4$ nmi) and that five more might appear ($\lambda_{E(1)} = 4.4$ nmi, $\lambda_{E(3)} = 2.0$ nmi, $\lambda_{E(8)} = 6.3$ nmi, $\lambda_{E(9)} = 2.2$ nmi, and $\lambda_{E(10)} = 4.1$ nmi). Several of the latter five layers require an increase in shear only slightly greater than $\Delta(\partial V/\partial z)$ for $Ri_{MIN} < 0.25$. The isentropes in Fig. 15 show a distribution of observed waves approximately as indicated in Table I. Most of the waves are between about 0.8 and 2.3 nmi, with several between 4 and 5 nmi. These wavelengths agree well with the expected values except for $\lambda_{E(8)} = 6.3$ nmi and $\lambda_{E(7)} = 0.4$ nmi. The potential temperature for the latter layer was calculated to be $\theta \leftarrow 483$ K and, judging by the potential temperatures shown in Fig. 15, it is apparent that this layer did not come low enough in altitude to be in the region of the U-2 flights.

The small waves and turbulence in the isentropes appear to start near the upstream peak and to extend over at least the next two troughs and peaks. As indicated in Table I, the initial shears were both positive and negative so that the small waves would be expected at peaks and also in troughs.

It is also interesting to compare the middle group of isentropes in Fig. 15 with the predictions shown in Table I. All five layers in this altitude range were predicted to remain stable even under the most pessimistic of assumptions, i.e., using $2\Delta(\partial V/\partial z)$ in computing Ri_{MIN}. No small waves are indicated in Fig. 15. Dr. Lilly has subsequently indicated that flights were made through this region at four levels; no small waves were observed in reducing the data, and the pilots did not report turbulence.

Concluding Remarks

The preceding results appear to confirm that very stable layers in the atmosphere can be destabilized by increases in shear caused by mountain lee waves. Moreover, it has been shown that stability criteria such as that of Drazin can be used to predict the onset of instability, the approximate wavelengths that would occur, and the locations of the small waves and turbulence.

This flow phenomenon undoubtedly occurs at all altitudes (not only in the stratosphere). As indicated previously, billow clouds of the non-convective variety are frequent evidence of the phenomenon occurring in the troposphere. It need not be associated with orographic disturbances. Shear-gravity waves (Ref. 28) can be created wherever a major inversion and strong wind shear occur, such as is often the case at the tropopause. These waves have wavelengths and amplitudes similar to those

of mountain waves and can cause similar increases in shear within stable layers. The phenomenon can also occur when stable layers flow over the tops of large cumulonimbus clouds.

Thus, the phenomenon could be responsible for an appreciable fraction of clear air turbulence encounters.

REFERENCES

1. Baumeister, T., ed.: Marks' Mechanical Engineers' Handbook. Sixth Edition, McGraw-Hill Book Company, Inc., New York, 1958.

2. Hama, F. R.: Streaklines in a Perturbed Shear Flow. The Physics of Fluids, Vol. 5, No. 6, June 1962, pp. 644-650.

3. Drazin, P. G. and L. N. Howard: Hydrodynamic Stability of Parallel Flow of Inviscid Fluid. Advances in Applied Mechanics, Vol. 9, published by Academic Press, New York, 1966, pp. 1-89.

4. Drazin, P. G.: The Stability of a Shear Layer in an Unbounded Heterogeneous Inviscid Fluid. Journal of Fluid Mechanics, Vol. 4, 1958, pp. 214-224.

5. Drazin, P. G. and L. N. Howard: The Instability to Long Waves of Unbounded Parallel Inviscid Flow. Journal of Fluid Mechanics, Vol. 14, 1962, pp. 257-283.

6. Miles, J. W. and L. N. Howard: Note on a Heterogeneous Shear Flow. Journal of Fluid Mechanics, Vol. 20, 1964, pp. 331-336.

7. Businger, J. A.: On the Energy Supply of Clear Air Turbulence. Symposium on Clear Air Turbulence and Its Detection; Boeing Scientific Research Laboratories Report D1-82-0740, Seattle, Washington, August 1968.

8. Schlichting, H.: Boundary Layer Theory. Pergamon Press, Ltd., London, 1955, pp. 357-359.

9. Michalke, A.: On Spatially Growing Disturbances in an Inviscid Shear Layer. Journal of Fluid Mechanics, Vol. 23, 1965, pp. 521-544.

10. Freymuth, P.: On Transition in a Separated Laminar Boundary Layer. Journal of Fluid Mechanics, Vol. 25, 1966, pp. 683-704.

11. Huschke, R. E.: Glossary of Meteorology. American Meteorological Society, Boston, Massachusetts, 1959.

12. Hazel, P.: Instabilities of Stratified Shear Flow. Paper submitted for publication in Journal of Fluid Mechanics, 1968.

13. Woods, J. D.: Wave-Induced Shear Instability in the Summer Thermocline. Journal of Fluid Mechanics, Vol. 32, 1968, pp. 791-800.

14. Woods, J. D.: CAT Under Water. Weather, Vol. XXIII, No. 6, June 1968, pp. 224-235.

15. Woods, J. D. and G. G. Fosberry: The Structure of the Thermocline. Underwater Association Report 1966-1967, published by T.G.W. Industrial and Research Promotions, Ltd., pp. 6-18.

16. Woods, J. D.: An Investigation of Some Physical Processes Associated with the Vertical Flow of Heat Through the Upper Ocean. Meteorological Magazine, Vol. 97, 1968, pp. 65-72.

17. Phillips, O. M.: The Dynamics of the Upper Ocean. Cambridge University Press, 1966.

18. Ludlam, F. H.: Characteristics of Billow Clouds and Their Relation to Clear Air Turbulence. Quarterly Journal of the Royal Meteorological Society, Vol. 93, 1967, pp. 419-435.

19. Mitchell, F. A. and D. T. Prophet: Meteorological Analysis of Clear Air Turbulence in the Stratosphere. Symposium on Clear Air Turbulence and Its Detection; Boeing Scientific Research Laboratories Report D1-82-0740, Seattle, Washington, August 1968.

20. Spillane, K. T.: Clear Air Turbulence and Supersonic Transport. Nature, Vol. 214, No. 5085, April 15, 1967, pp. 237-239.

21. Hardy, K. R.: Radar Echoes from the Clear Air. Paper prepared for NATO Advanced Study Institute on the Structure of the Lower Atmosphere and Electromagnetic Wave Propagation, Aberystwyth, Wales, September 2-15, 1967.

22. Stewart, R. W.: Comments during panel discussion at Boeing Scientific Research Laboratories Symposium on Clear Air Turbulence and Its Detection, Seattle, Washington, August 14-16, 1968.

23. Nicholls, J. M.: Conference at United Aircraft Research Laboratories, April 15, 1969.

24. Nicholls, J. M.: Meteorological Office Letter to J. W. Clark, United Aircraft Research Laboratories, May 28, 1969.

25. McPherson, A. and J. M. Nicholls: Results of a Series of Flights in the Stratosphere over Mountainous Terrain in the Western U.S.A. during February 1967. To be published as an R.A.E. Technical Report, 1969.

26. Zalkan, R. L.: Observation of High Frequency Internal Waves in the Ocean. Scripps Institution of Oceanography, Marine Physical Laboratory Report SIO Reference 68-28, September 1968.

27. Lilly, D. K.: Lee Waves in the Colorado Rockies. Symposium on Clear Air Turbulence and Its Detection; Boeing Scientific Research Laboratories Report D1-82-0740, Seattle, Washington, August 1968.

28. Haurwitz, B.: Dynamic Meteorology. McGraw-Hill Book Company, Inc., New York, 1941.

29. Schubauer, G. B. and H. K. Skramstad: Laminar Boundary Layer Oscillations and Stability of Laminar Flow. Journal of the Aeronautical Sciences, Vol. 14, No. 2, February 1947, pp. 69-78.

30. Rayleigh, Lord: Scientific Papers, Vol. IV. Cambridge University Press, 1916.

31. Ludweig, H.: Stability of Flow in an Annular Space. Zeitschrift für Flugwissenschaften, Vol. 8, 1960, pp. 135-140.

32. McLean, G. S. and R. M. Endlich: Empirical Relationships Between Gust Intensity in Clear Air Turbulence and Certain Meteorological Quantities. AFCRL-65-635, Environmental Research Papers No. 132, 1965.

33. George, J. J.: A Case History of Clear Air Turbulence. Eastern Airlines, Inc., 1967.

34. Helvey, R. A.: Observations of Stratospheric Clear-Air Turbulence and Mountain Waves over the Sierra Nevada Mountains. U.S.A.F. Report AFCRL-68-0001, prepared by UCLA Department of Meteorology, December 1967.

LIST OF SYMBOLS

a	Amplitude of wave (half the height from trough to peak), ft or in.
b	Exponent in theoretical velocity profile (Fig. 10), dimensionless
c	Complex wave velocity, $c = c_r + i\, c_i$, ft/sec
c_i	Imaginary part of complex wave velocity, ft/sec
c_r	Real part of complex wave velocity, ft/sec
d	Shear-layer scale length, $d = (\Delta V/2)/(\partial V/\partial z)$, ft
d_1	Distance from surface to thermocline in water channel, ft
d_2	Distance from thermocline to channel floor, ft
E	Anemometer output voltage, v
g	Gravitational constant, 32.2 ft/sec^2
i	Unit imaginary number, $\sqrt{-1}$, dimensionless
k	Wavenumber of shear-gravity wave, $k = 2\pi/\lambda_{SW}$, ft^{-1}
ℓ	Unit length, ft
n	Wave frequency, $2\pi V_o/\lambda_{LW}$, sec^{-1}; also coordinate normal to isobars or isotherms, nmi
N_M	Brunt-Väisälä frequency, $N_M = \sqrt{(g/T_o)\cdot\left[(\partial T/\partial z) - (\partial T/\partial z)_{ad}\right]}$ in the atmosphere and $\sqrt{(-g/\rho)(\partial\rho/\partial z)}$ in the water channel, sec^{-1}
P	Pressure, mb
r	Radial coordinate measured from center of curvature of water channel, ft or in.
Re	Reynolds number, $Re = V\ell/\nu$, dimensionless
Ri	Richardson number, $Ri = \left[g/T_o\right]\left[(\partial T/\partial z) - (\partial T/\partial z)_{ad}\right]/\left[\partial V/\partial z\right]^2$ in the atmosphere and $\left[-g/\rho\right]\left[\partial\rho/\partial z\right]/\left[\partial V/\partial z\right]^2$ in the water channel, dimensionless

Ri_o	Initial or upstream Richardson number, dimensionless
Ri_{MIN}	Minimum Richardson number caused by influence of long-wavelength wave, dimensionless
s	Coordinate along centerline of curved water channel (Fig. 2), ft or in.
t	Time, sec
T	Temperature, deg C, K, or F
T_o	Temperature at center of shear layer, deg C, K, or F
V	Velocity, ft/sec or kts
V_o	Velocity at center of shear layer, ft/sec or kts
V_1, V_2	Velocities in upper and lower streams bounding shear layer, respectively, ft/sec
x	Downstream coordinate in water channel (Fig. 2), ft or in.; also distance along flight path, nmi
y	Transverse coordinate in water channel (Fig. 2), ft or in.
z	Vertical coordinate in water channel (Fig. 2), ft or in.; also pressure altitude, ft
z_o	Vertical coordinate of center of shear layer in water channel, ft or in.
α	Wavenumber of small-amplitude waves associated with instabilities in shear layers, $\alpha = 2\pi/\lambda$, ft^{-1}
β	Parameter in density profile equation (Eq. (2)), $\beta = Ri \cdot d \cdot (\partial V/\partial z)_o^2/g$, dimensionless
ΔV	Velocity difference across shear layer, $\Delta V = V_1 - V_2$, ft/sec
$\Delta(\partial V/\partial z)$	Change in shear caused by influence of long-wavelength wave, sec^{-1}
$(\partial T/\partial z)_{ad}$	Adiabatic lapse rate, $(\partial T/\partial z)_{ad} = -2.98 \times 10^{-3}$ deg C/ft

$(\partial V/\partial z)_o$	Initial or upstream shear, sec^{-1} or kts/1,000 ft
ϵ	Thickness of thermocline, ft
η	Parameter in analysis of shear-layer instability induced by shear-gravity waves, $\eta = (k\epsilon/2) \cdot \tanh (kd_1)$, dimensionless
θ	Potential temperature (see Appendix III), deg K
λ	Wavelength of small-amplitude waves associated with instabilities in shear layers, ft or in.
$\lambda_{E(\ )}$	Wavelength of instability estimated to occur in atmospheric shear layer (number in brackets identifies layer), ft or nmi
λ_{LW}	Wavelength of lee wave, ft or nmi
λ_o	Wavelength of instability observed in atmospheric shear layer, ft or nmi
λ_{SW}	Wavelength of shear-gravity wave in water channel, ft or in.
ν	Kinematic viscosity, ft^2/sec
ρ	Density of water or air, $slugs/ft^3$
ρ_o	Density of water or air at center of shear layer, $slugs/ft^3$
ρ_1, ρ_2	Densities in upper and lower streams bounding shear layer, respectively, $slugs/ft^3$
$\phi(z)$	Perturbation amplitude function in shear-layer stability analysis, ft^2/sec
ψ'	Perturbation stream function in shear-layer stability analysis, ft^2/sec

APPENDIX I

SUMMARY OF OTHER FLUID MECHANICS EXPERIMENTS

Experiments with an Oscillating Plate to Induce Disturbances in a Shear Layer

The data in Fig. 9 indicate that the downstream distances at which waves, vortices and turbulence were first observed were strongly dependent upon the shear. Attempts were made to induce disturbances in the shear layer so as to promote transition from waves to vortices further upstream. This was done using an oscillating plate which in principle was analogous to the vibratory ribbon used by Schubauer and Skramstad in their boundary layer experiments (Ref. 29).

The 0.015-in.-thick plate had a chord of 0.5 in. and a span of 23.5 in. It was supported at the ends and midspan by rods connected to a frame which ran transversely above the surface of the water. The plate was positioned 10 in. downstream of the filter bed at a height such that it was near the center of the shear layer. The plate was oscillated in the vertical direction by an electromagnetic vibrator at frequencies from 0.005 to 2 cps. This allowed a large range of the nondimensional wavenumber to be investigated ($0 < \alpha d < 2$). At the lower frequencies, the amplitude was on the order of a quarter of an inch, and the waves that were generated appeared similar to the one shown in Fig. 5(b).

Although the results were not entirely consistent, in the tests with $Ri < 0.25$, the location of transition to vortices tended to move upstream of its natural location when the forced αd was close to the natural αd. Also, it was observed that instabilities could not be induced in tests with $Ri > 0.25$.

Experiments with Standing Shear-Gravity Waves

Standing shear-gravity waves of the type discussed by Haurwitz (Ref. 28) were also studied using the water channel. These waves occur when two adjacent streams have different velocities and densities (the lighter stream being on top). The wavelength is given by

$$\lambda_{SW} = \frac{2\pi V_2^2}{g(1-\rho_1/\rho_2)}\left[\left(\frac{V_1}{V_2}\right)^2 \cdot \frac{\rho_1}{\rho_2} + 1\right] \qquad (12)$$

where the subscripts 1 and 2 denote the upper and lower layers, respectively. In the channel, the observed wavelengths were from 12 to 24 in. and the amplitudes (half the height from trough to peak) were as much as 1.5 in.

The primary reason for investigating these waves was to examine the phenomenon discussed in the main text, that is, the situation where initially stable layers are destabilized by the increase in shear near the peaks and troughs of long-wavelength waves.

The flow conditions and wave parameters which must exist for local instability of the flow caused by reinforcement of the initial shear at a crest or a trough are described using two inequalities. The first is

$$Ri_0 = \frac{N_M^2}{\left(\frac{\partial V}{\partial z}\right)_0^2} > 0.25 \tag{13}$$

where $N_M^2 = (-g/\rho)(\partial\rho/\partial z)$. This inequality states that the initial shear $(\partial V/\partial z)_0$, the density gradient $\partial\rho/\partial z$, and the mean density ρ, must be such that the flow upstream of the shear-gravity wave is stable. The second inequality is

$$Ri_{MIN} = \frac{N_M^2}{\left[|(\partial V/\partial z)_0| + \Delta(\partial V/\partial z)\right]^2} < 0.25 \tag{14}$$

This states that the initial shear, the wave shear $\Delta(\partial V/\partial z)$, the density gradient and mean density must be such that the flow with the shear-gravity wave is unstable locally. Inequalities (13) and (14) can be combined to obtain

$$2N_M - \Delta(\partial V/\partial z) < |(\partial V/\partial z)_0| < 2N_M \tag{15}$$

Thus, the required conditions for the flow to be locally unstable are that the initial shear be between twice the Brunt-Väisälä frequency and twice the Brunt-Väisälä frequency minus the wave shear. One further relationship is needed to define the wave shear in terms of the flow conditions and wave parameters. From Ref. 17, which considered gravity waves in the ocean, the following can be derived:

$$\Delta(\partial V/\partial z) = \frac{2N_M}{\eta + 1} \tag{16}$$

where $\eta = (k\epsilon/2)\cdot\tanh(kd_1)$, k is the shear-gravity wave wavenumber ($k = 2\pi/\lambda_{SW}$), ϵ is the thickness of the thermocline, and d_1 is the distance from the surface of the flow to the thermocline. The distance from the thermocline to the channel floor would be d_2. In the water channel experiments, $d_1 \approx d_2$. Substitution of Eq. (16) into Eq. (15) results in

$$\left[1 - \frac{1}{\eta+1}\right] \cdot 2N_M < |(\partial V/\partial z)_o| < 2N_M \tag{17}$$

This inequality has been shown graphically in Fig. 17 in a form which allows interpretation of the experimental observations.

In Fig. 17, the ordinate is the absolute value of the initial shear, $|(\partial V/\partial z)_o|$, and the abscissa is the Brunt-Väisälä frequency, N_M. The lines emanating from the origin are lines of constant η for values of η close to the values at which observations were made in the channel. For the value of η indicated on any given line, the flow would be locally unstable due to the presence of the shear-gravity wave only if the experimental point N_M, $|(\partial V/\partial z)_o|$ falls between that line and the line for $\eta = \infty$. This locally unstable region widens as η decreases. If an experimental point falls outside this region and in the upper left-hand corner, then the flow would have been unstable even without the shear-gravity wave because the upstream value of the Richardson number was less than 0.25. If the experimental point falls outside this region and in the lower right-hand corner, then the flow would remain stable because even with the wave, the Richardson number was not decreased enough to become less than 0.25.

The experimental points are also shown in Fig. 17. The solid symbols denote conditions at which no shear-gravity waves were observed. The open symbols denote conditions at which shear gravity waves were observed, and the number adjacent to the symbol indicates the experimental value of η.

The only point at which both shear-gravity waves and an instability in the shear layer were observed was at $N_M = 0.57$, $|(\partial V/\partial z)_o| = 1.32$, $\eta = 0.8$; this point is denoted by an asterisk in Fig. 17. A photograph of the bubble traces immediately downstream of the filter bed is shown in Fig. 18(a). A photograph showing the vortices which formed downstream of the first trough is shown in Fig. 18(b). It will be noted in Fig. 17 that this point is just over the $\eta = \infty$ line and in the region of unstable flow upstream. Therefore, it is questionable whether this is a genuine case of a shear layer being destabilized by a shear-gravity wave.

Taking into consideration other factors which affect the characteristics of the shear-gravity waves that can be established in the channel, it has been decided to group the hot-water nozzles (Fig. 2) closer together in future tests. This should provide thinner thermoclines (hence, smaller experimental values of η), thereby increasing the probability of obtaining flow conditions that are inside the region of locally unstable flow.

Experiments with the Channel Walls Curved

Experiments were also conducted with the channel side walls curved. The objectives of this portion of the study were to investigate isothermal flows with curvature and to compare the results with existing theoretical stability criteria for rotating flows. For the reasons outlined below, suitable data could not be obtained for these purposes.

Theoretical criteria such as those of Rayleigh and Ludwieg (Refs. 30 and 31) indicate that the parameter $(r/V)/(\partial V/\partial r)$ is important for stability. The Rayleigh criterion states that the flow should be stable for $-1 < (r/V)/(\partial V/\partial r)$. The Ludwieg criterion predicts the same except for a neutrally stable point at $(r/V)/(\partial V/\partial r) = +1$.

Accordingly, the initial experiments were conducted so as to examine flows ranging from -4 to +5 or 6. For these tests, $\partial V/\partial z \approx 0$. Transverse shears in the range $-0.04 < \partial V/\partial r < +0.04$ sec^{-1} were obtained by tapering the filter bed uniformly across the channel. Most of these flows showed some unsteadiness, particularly near the downstream end of the channel, although turbulence such as that shown in Fig. 5(d) was not seen. When flow conditions were repeated, the dye traces did not always appear the same. Thus, these tests were inconclusive.

Tests were subsequently conducted with much larger shears. These were established using filter beds that had a constant thickness over most of the left side of the channel, a different thickness over most of the right side, and a ramp section in between (similar to the filter bed section shown in the sketch in Fig. 5, only in the x-y plane. The flow therefore had a transverse shear layer similar to the vertical shear layers that were studied (Fig. 5), and the flow patterns during breakdown were also similar.

The principal result is shown in Fig. 19. The locations at which the first waves, vortices and turbulence were observed are shown for values of $\partial V/\partial r$ from -0.25 to +0.54 sec^{-1}. It is evident that as the shear approaches zero, the first observable waves occur further and further downstream. For these tests, $r/V = 100$ to 150; thus, all of the points shown are outside the region $-1 < (r/V)(\partial V/\partial r) < +1$ except the one at $\partial V/\partial r = 0$. This explains why the initial results are inconclusive and points out the relative difficulty of attaining the stated objectives in the 120-in.-long channel.

It will be noted in Fig. 19 that the trend lines are asymmetrical about $\partial V/\partial r = 0$. The instability is observed further upstream for negative shears (velocity decreasing radially outward) than for positive shears.

Preliminary tests were also conducted with transverse temperature gradients imposed using the vertical hot-water nozzles. The objective was to determine whether transverse gradients could in fact be established in the channel. The resulting flows were steady, although substantial vertical temperature gradients also occurred. The maximum transverse gradient in the tests was about $\partial T/\partial r = -4$ deg F/ft; this was accompanied by a vertical gradient of about $\partial T/\partial z = +35$ deg F/ft.

APPENDIX II

SUMMARY OF METEOROLOGICAL ANALYSES OF SIX CLEAR AIR TURBULENCE ENCOUNTERS*

Six different CAT cases from airline, military, and AFCRL-NASA experience were analyzed. The primary objectives of these analyses were: (1) to identify characteristic atmospheric flows associated with CAT for investigation in the fluid mechanics experiments, (2) to identify meteorological features associated with CAT and sources of instabilities in the atmosphere, (3) to determine which fluid mechanics parameters might be suitable as stability criteria, and (4) to obtain quantitative atmospheric data for comparison with laboratory data.

Method of Analysis

For the CAT cases selected, charts for sea level and all standard Cp levels between 850 mb and 150 mb --- higher in some cases --- were analyzed to show pressure gradients, wind and temperature fields. Frontal and tropopause intersections with these surfaces in and adjacent to the turbulent regions were located at standard hours before, during, and after the turbulence encounters. Information used in these analyses included data from research aircraft (Project Jet Stream, HICAT, AFCRL), airline flights (EAL and UAL), and rawinsondes obtained from the U. S. Weather Bureau at Ashville, N. C. Time and space cross sections through significant regions aided in the identification of discontinuities, jet steams, and other meteorological features. Auxiliary plots on the thermodynamic diagrams were prepared when necessary to locate inversions and instability layers, and for the calculation of specific parameters (i.e., Richardson numbers, etc.). Particular attention was given to front and tropopause analysis to achieve consistency from level to level and from time to time. Frontal and tropopause contour charts were found to be especially useful for analyzing the characteristics of these discontinuities.

Primary Results

Table II summarizes the flow conditions for all six cases. Figure 20 is an idealized cross section showing the turbulence regions relative to the fronts and tropopause.

---

* Prepared by E. Brewster Buxton, Consulting Meteorologist.

1. Project Jet Stream Flight 29 flown over New England on 4 April 1957

This flight was selected for study because (1) the flow was anticyclonic and (2) CAT was reported along a tropopause surface and at the frontal intersection on the north side of the jet stream. The well-instrumented B-47 provided a large amount of data at all levels which, when combined with routine RAOBs from the area, made it possible to analyze the principal circulation and thermal patterns. Significant features identified in the analysis of this case included:

(a) Evidence of turbulent eddies - VGH data
(b) Anticyclonic streamline curvature
(c) Density discontinuities --- tropopause and front
(d) Vertical motion and cooling --- rising tropopause
(e) Possible waves on tropopause surface
(f) Mountains below jet core
(g) High pressure ridge moving east
(h) Front moving northward.

2. Project Jet Stream Flight 27 flown over Georgia, 29 March 1957

In this case, moderate/severe turbulence was encountered at a point where the tropopause sloped downward to meet the polar front at 35,000 ft. The flow was cyclonic with a marked shift from northwest to southwest at the frontal intersection. Horizontal wind shear was the most significant feature in this case, reaching a value of 35 kts in 7 nmi, an extreme not exceeded in any other Project Jet Stream flight.

3. Severe CAT at Frontal Surface, Jacksonville, Florida, 29 November 1966

Four of five severe jolts in rapid succession (maximum 2.5 g, measured from 1.0 g datum) were encountered at 17,000 ft as the Electra aircraft cruised northward. Turbulence continued during descent into Jacksonville to 11,000 ft. The analysis indicates that the turbulence occurred on a sloping frontal surface. Between 17,000 and 11,000 ft in the vicinity of Jacksonville, the frontal slope was 1/80 and the layer was about 6,000 ft thick (stable layer). Farther north the front sloped sharply up to a vertical position joining with the tropopause at about 30,000 ft. The core of the jet stream was centered unusually low (between 22,000 and 25,000 ft) with a maximum wind estimated to be 175 kts.

The Cp charts indicated a sharp north-south trough with wind directions shifting from northwest to southwest in the vicinity of the CAT encounter. While CAT probably occurred along the frontal slope for several hundred miles, it is likely that the most severe turbulence was associated with the wind directional shear at the trough.

4. UAL CAT Incident, Wyoming, 29 March 1967

Severe CAT was encountered at 37,000 ft about 40 nmi southwest of Crazy Woman VOR in Wyoming by a United Air Lines flight on an eastbound course at 1937 GMT.

This case was selected for analysis because of its assumed relationship to mountain wave conditions. However, upon analysis it appears that the turbulence encountered was associated more directly with a tropopause boundary near its intersection with the polar front. In the region of the turbulence, between 34,000 and 38,000 ft an unusually steep gradient on the stratospheric side of the sloping tropopause boundary (8 C in 160 nmi) prevailed. Evidence of mountain wave activity is also available but may not by itself account for the CAT.

Several synoptic features commonly associated with CAT were present on the date of this incident:

(a) A deep trough of low pressure west of the Rockies producing a strong flow of winds at right angles to mountains in Wyoming, with the core of the jet stream at 34,000 ft (130 kts);

(b) A deepening cyclone on the polar front, occluding as it moved northward over Utah and Wyoming into Montanna with active fronts;

(c) Steeply sloping tropopause surface over the Pacific Northwest, dipping from 38,000 ft over the Dakotas, intersecting the Polar Front at 32,000 ft over Utah and dipping further to 26,000 ft over Washington and Oregon. In this situation, the tropopause surface was changing rapidly in height as a result of well-defined waves on the surface.

5. CAT Detected by Multiwavelength Radar at NASA Wallops Island, Virginia, 28 February 1968

The significant association of CAT patches with clear-air echoes detected by sensitive vertically pointed radars has been reported by K. R. Hardy and colleagues at AFCRL. Because of the fine-scale resolution of radar returns, the supporting aircraft observations and the special rawinsonde data obtained in the AFCRL tests at NASA Wallops Island, one of the cases of moderate-to-severe turbulence which occurred in the vicinity of the tropopause was examined with the object of determining further characteristics of the tropopause in the regions of CAT.

These analyses showed the structure of the fronts involved and the configuration of the tropopause surface 6 hours before and 6 hours after the CAT observations. No definite wave forms on the tropopause surfaces were evident. The position of the tropopause and frontal surfaces over NASA Wallops Island, and their slopes, were confirmed by consistency and continuity between the various charts analyzed.

The meteorological situation in this case was complex with occluded waves on the polar front in very low latitudes resulting in bent-back occlusions, secondary fronts and double jet maxima. It is likely that CAT occurred on some of these fronts, but the test data was obtained locally in the vicinity of NASA Wallops Island at levels above the fronts at the tropopause.

6. Stratospheric CAT and Mountain Waves Over California, 15 May 1964

The tropopause was the only discontinuity in the region of the flights (polar front and jet core were over Oregon and Washington). The flow over the mountains was southwesterly in the troposphere, reaching a maximum of approximately 80 kts just below the tropopause at 41,000 ft and decreasing to 30 kts in a deep inversion layer above the tropopause which extended to above 70,000 ft. The flow was anticyclonic at all levels above 20,000 ft.

No significant frontal displacements occurred during the 24 hours preceding these flights, and the tropopause remained at the same pressure altitude (41,000 ft). Waves detected by analysis of U-2 traverses in the stratosphere (isentropic streamlines) appear to have been initiated by mountain waves produced below.

Horizontal temperature gradients in the stratosphere were weak above the portion of the tropopause which was nearly horizontal, but steepened sharply north of the area in Oregon and Washington where the tropopause dipped sharply downward to intersect the polar front at 300 mb over Seattle and Spokane. This strong gradient in the stratosphere over the sloping portion of the tropopause has been noticed in other cases studied (i.e., UAL Wyoming case) and is believed to be characteristic of horizontal (Cp) temperature patterns over jet streams.

Considering the relatively inactive synoptic situation and the weak shears present, the turbulence reported is judged to be associated with mountain wave activity.

APPENDIX III

GLOSSARY OF PRINCIPAL METEOROLOGICAL TERMS

adiabatic lapse rate - The rate of decrease of temperature with height of a parcel of dry air lifted adiabatically through an atmosphere in hydrostatic equilibrium. The rate of change of pressure with height is $\partial P/\partial z = -g\rho$ and the adiabatic lapse rate is $(\partial T/\partial z)_{ad} = -(g/\gamma R)(\gamma - 1) = -2.98 \times 10^{-3}$ deg C/ft, where R is the gas constant and γ is the ratio of specific heats. Note that a minus sign is used in this report for all cases where temperature decreases with altitude.

Brunt-Väisälä frequency - The natural frequency of oscillation of a vertical column of fluid given a small displacement from its equilibrium position. In the water channel, $N_M^2 = -(g/\rho)(\partial\rho/\partial z)$; in the atmosphere, $N_M^2 = (g/T_o) \cdot \left[(\partial T/\partial z) - (\partial T/\partial z)_{ad} \right]$.

environmental lapse rate - The rate of change of temperature with height in the atmosphere, $(\partial T/\partial z)$. In this report, a minus sign is used for all cases where temperature decreases with altitude.

isentrope - A line of constant potential temperature.

mountain wave, lee wave - A gravity wave disturbance which is caused by, and stationary with respect to, a barrier in the flow such as a mountain range.

potential temperature - The temperature a parcel of dry air would have if brought adiabatically from its initial state to the arbitrarily selected standard of 1000 mb. The equation for potential temperature is $\theta = T(1000/P)^{(\gamma-1)/\gamma}$.

Radiosonde - A balloon-borne instrument for the simultaneous measurement and transmission of meteorological data.

shear-gravity wave - A combination of gravity waves and Helmholtz waves on a surface of discontinuity of density and velocity. The density difference contributes to stability and the velocity difference to instability.

stratosphere - The atmospheric shell extending upward from the tropopause to the altitude at which temperature begins to increase with increasing altitude (82,021 ft in the ICAO Standard Atmosphere).

thermocline - A vertical temperature gradient in some layer of a body of water which is appreciably greater than the gradients above and below it. Also, a layer in which such a gradient occurs.

tropopause - The boundary between the troposphere and stratosphere, usually characterized by an abrupt change from less stable to more stable lapse rates (36,089 ft in the ICAO Standard Atmosphere).

TABLE I

CHARACTERISTICS OF EXPECTED AND OBSERVED SMALL-WAVELENGTH WAVES
FOR CALIFORNIA AND COLORADO LEE WAVE CASES

		EXPECTED WAVES									OBSERVED WAVES		
								Based on $\Delta(\partial V/\partial z)$		Based on $2\Delta(\partial V/\partial z)$			
Case	Stable Layer	Mean Altitude, ft	θ, deg K	Thickness, 2d - ft	$\lambda_{E(\ )}$, nmi	Expected Location in Lee Waves	Ri_o	Ri_{MIN}	Waves Likely? ($Ri_{MIN} < 0.25$?)	Ri_{MIN}	Waves Likely? ($Ri_{MIN} < 0.25$?)	Waves Observed?	λ_O, nmi	Location in Lee Waves
California	1	41,900	354	2,600	1.9	peak	77.6	0.28	no(2)	0.07	yes	yes	1.9	after peak
	2	37,550	334	900	0.7	trough	8.7	0.52	no	0.17	yes		0.9-1.3	trough
Colorado(1)	1	60,718	451	6,000	4.4	trough	5.4	0.36	no(3)	0.12	yes			
	2	62,108	461	3,200	2.4	trough	3.5	0.20	yes	0.06	yes			
	3	59,114	440	2,800	2.0	trough	10.4	0.62	no	0.20	yes			
	7	67,195	483	600	0.4	peak	486.7	0.20	yes	0.05	yes	yes	35%:0.8-1.2; 50%:1.2-1.8; 15%:1.8-2.3; several between 4-5	appear to start at peak and extend downstream through at least two troughs and two peaks
	8	59,232	446	8,600	6.3	trough	26.5	0.61	no	0.18	yes			
	9	62,021	465	3,000	2.2	peak	757.9	0.33	no(4)	0.08	yes			
	10	57,715	435	5,600	4.1	trough	4.9	0.46	no	0.16	yes			
	4	47,112	389	700	0.5	trough	1.1	0.48	no	0.27	no	no - pilots reported very little or no turbulence.		
	5	43,055	366	1,300	1.0	trough	2.2	0.59	no	0.27	no			
	6	38,964	339	2,600	1.9	peak	2.6	0.83	no	0.40	no			
	11	43,475	375	1,300	1.0	trough	83.1	1.66	no	0.48	no			
	12	37,967	344	3,500	2.0	trough	158.9	5.09	no	1.63	no			

(1) Layers 1-6 from Granby radiosonde; layers 7-12 from Denver radiosonde.
(2) Yes for 6% greater $\Delta(\partial V/\partial z)$.
(3) Yes for 27% greater $\Delta(\partial V/\partial z)$.
(4) Yes for 15% greater $\Delta(\partial V/\partial z)$.

TABLE II

ATMOSPHERIC CONDITIONS ASSOCIATED WITH CLEAR AIR TURBULENCE CASES INVESTIGATED

	-1- Project Jet Stream Flt 29 New England 4 Apr, 1967	-2- Project Jet Stream Flt 27 Georgia 29 Mar, 1957	-3- EAL Jacksonville, Fla. 29 Nov, 1966	-4- UAL Wyoming 29 Mar, 1967	-5- Wallops Island Radar Tests 28 Feb, 1968	-6- U-2 Stratospheric Probes California 15 May, 1964
Flow Pattern	Anticyclonic Jet Core WNW 170 kts 36,000 ft PA	Cyclonic Jet Core SW 145 kts 37,000 ft PA	Cyclonic Jet Core West 165 kts 20,000 ft PA	Anticyclonic Jet Core SWly 130 kts 34,000 ft PA	Cyclonic Jet Core Wly 136 kts 30,000 ft PA	Anticyclonic Jet Core WSW 120 kts 32,000 ft PA
Meteorological Features	Tropopause and Polar Front	Tropopause Polar Front Intersection	Polar Front	Tropopause	Tropopause	Tropopause
Possible Source of Instability	Gravity waves on discontinuity surface. Moving Front and Trop.	Shear-Gravity Waves	Shear-Gravity Waves	Gravity waves in stable layer above Tropopause	Waves on Tropopause	Gravity waves on Trop. induced by mountains
Significant Parameters	Vertical Wind Shear. Possible Dynamic Instability.	Hor. Wind Shear Vert. Wind Shear Possible Dynamic Instability	Vert. Wind Shear, Inversion	Strong hor. temp. gradient 5,000 ft inversion layer above Trop. Rapidly changing front and Trop. contours	Inversion 10,000 + ft	Strong temp. gradient in stratosphere north of flight area
Quantitative Data dV/dz	-0.023 sec^{-1}	-0.03 sec^{-1}	0.06 sec^{-1}	-0.02 sec^{-1}	-0.037 sec^{-1}	-0.003 sec^{-1} Troposphere; 0.006 sec^{-1} Stratosphere
|dV/dn|	0.00004 sec^{-1} (15 kts/100 nmi); 0.0005 sec^{-1} (2 kts/nmi) at Front	0.0013 sec^{-1} (35 kts/7 nmi)	0.0004 sec^{-1} (1.6 kts/nmi)	Negligible	0.000035 sec^{-1} (0.13 kts/nmi)	0.00002 sec^{-1} (20 kts/240 nmi)
|dT/dn|	0.08 C/nmi 1.6 C/nmi (local)	0.25 C/nmi	0.2 C/nmi	0.05 C/nmi	0.05 C/nmi	0.02 C/nmi
dT/dz	0 to +2 C/1000 ft	Isothermal	+0.6 C/1000 ft	+1 C/1000 ft (5000-ft layer); then isothermal	Isothermal to 40,000 ft; then 1 C/1000 ft	Inversion +0.3 C/1000 ft
Coriolis Parameter	0.0001 sec^{-1}	0.000078 sec^{-1}	0.00007 sec^{-1}	0.0001 sec^{-1}	0.000085 sec^{-1}	0.000085 sec^{-1}
Primary Source of Information	Ref. 32	Ref. 32	Ref. 33	United Air Lines	AFCRL	Ref. 34

FIG. 1

PHOTOGRAPH OF UARL WATER CHANNEL

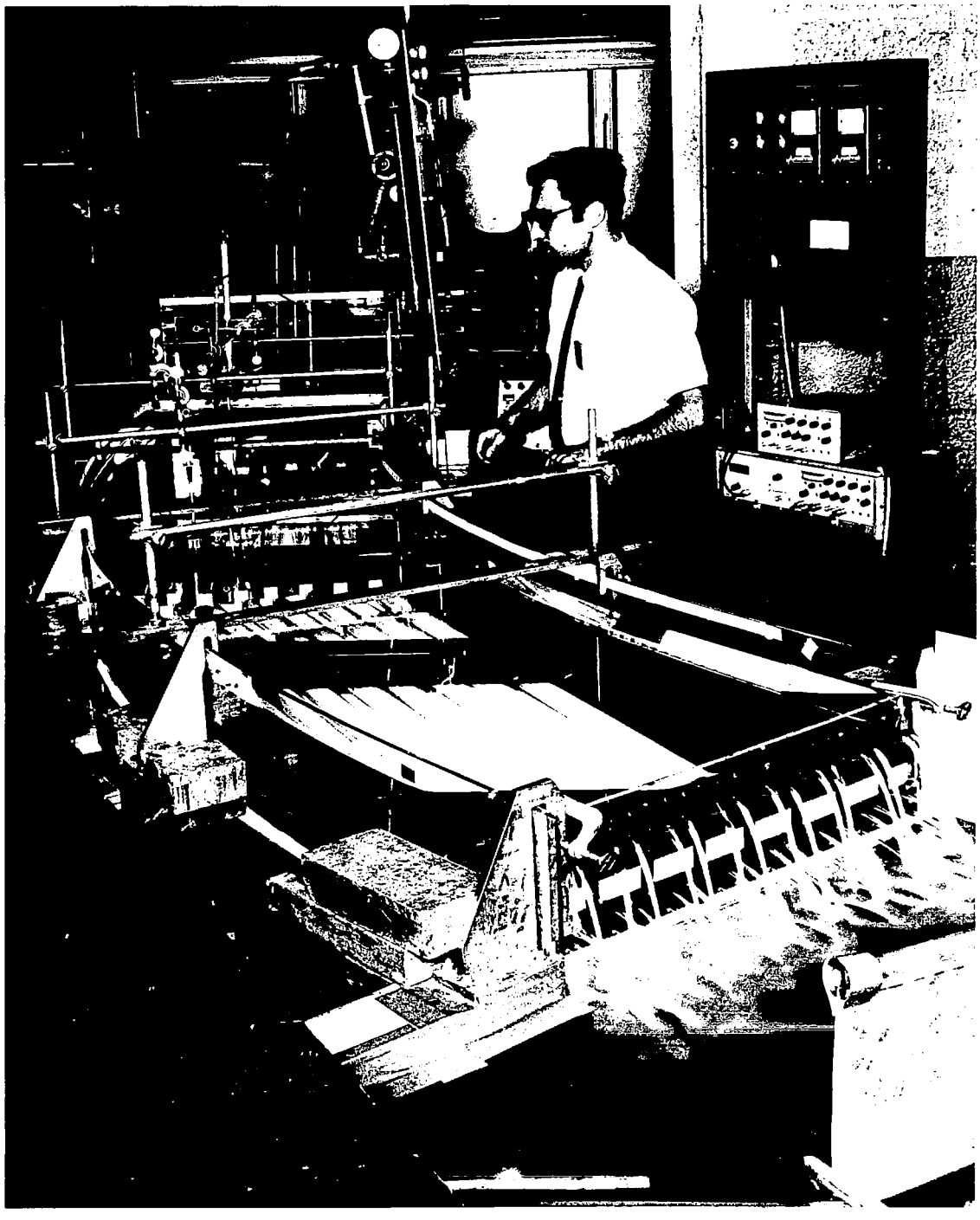

SKETCH OF UARL OPEN WATER CHANNEL

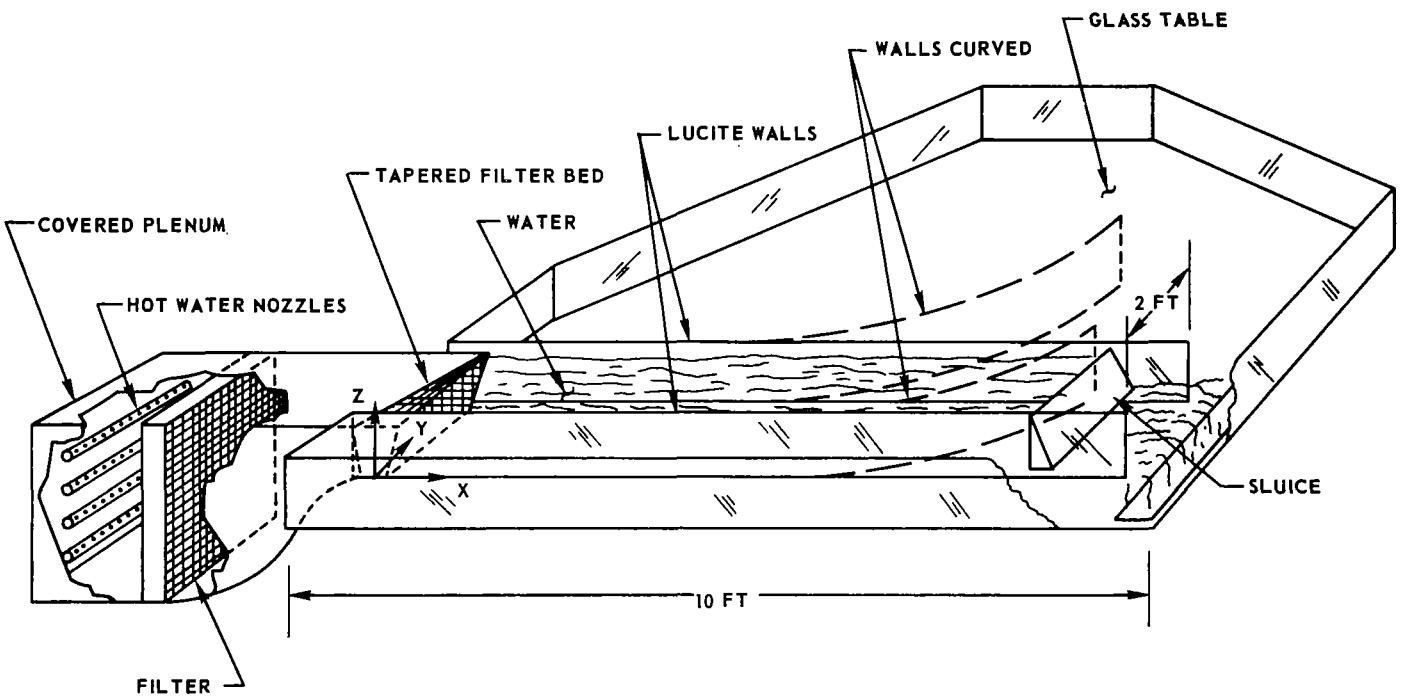

FIG. 2

FIG. 3

EFFECT OF TEMPERATURE ON PROPERTIES OF WATER

DERIVED FROM DATA IN REF. 1

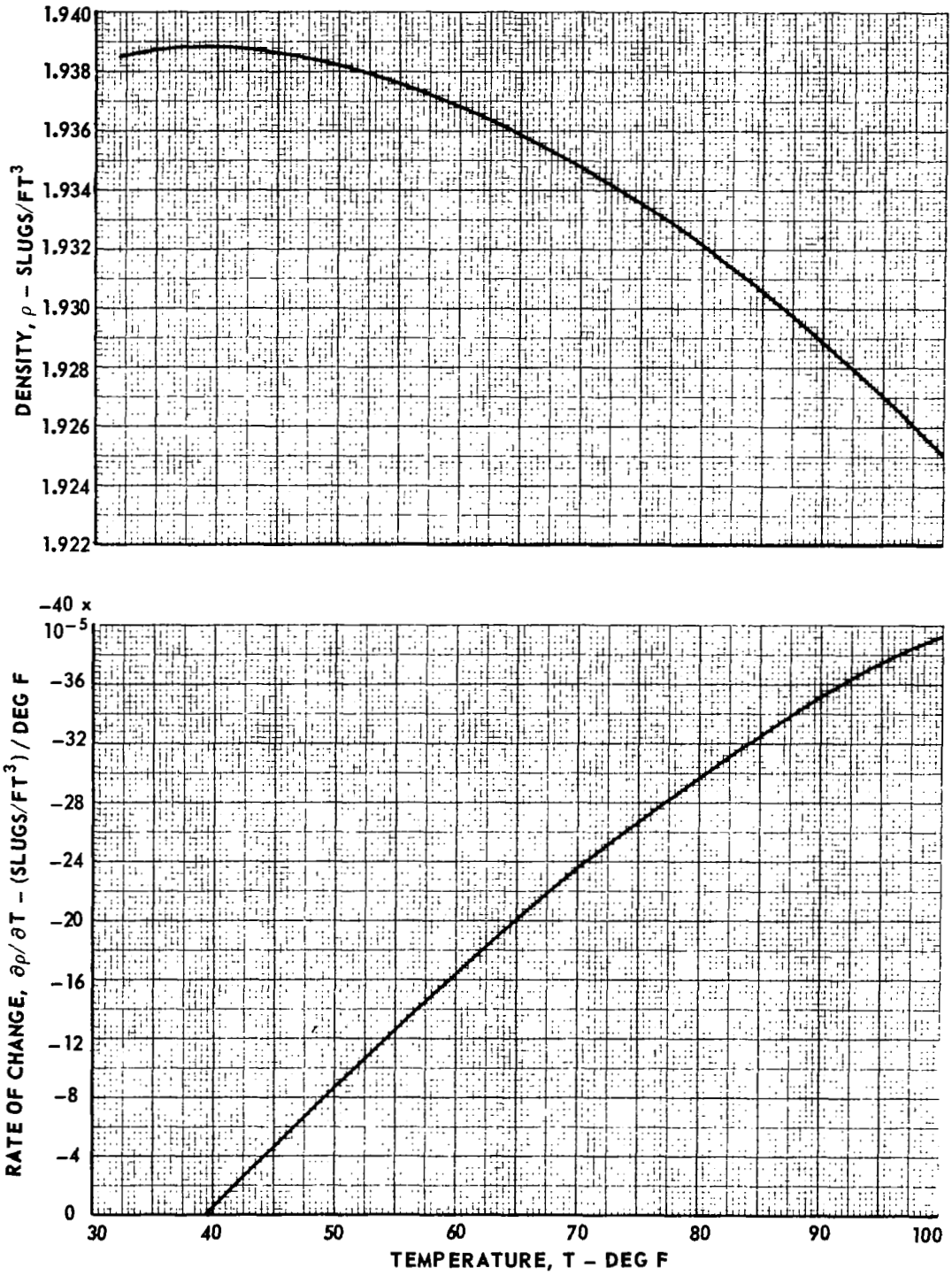

FIG. 4

TYPICAL VELOCITY, TEMPERATURE AND DENSITY PROFILES FOR SHEAR-LAYER EXPERIMENTS

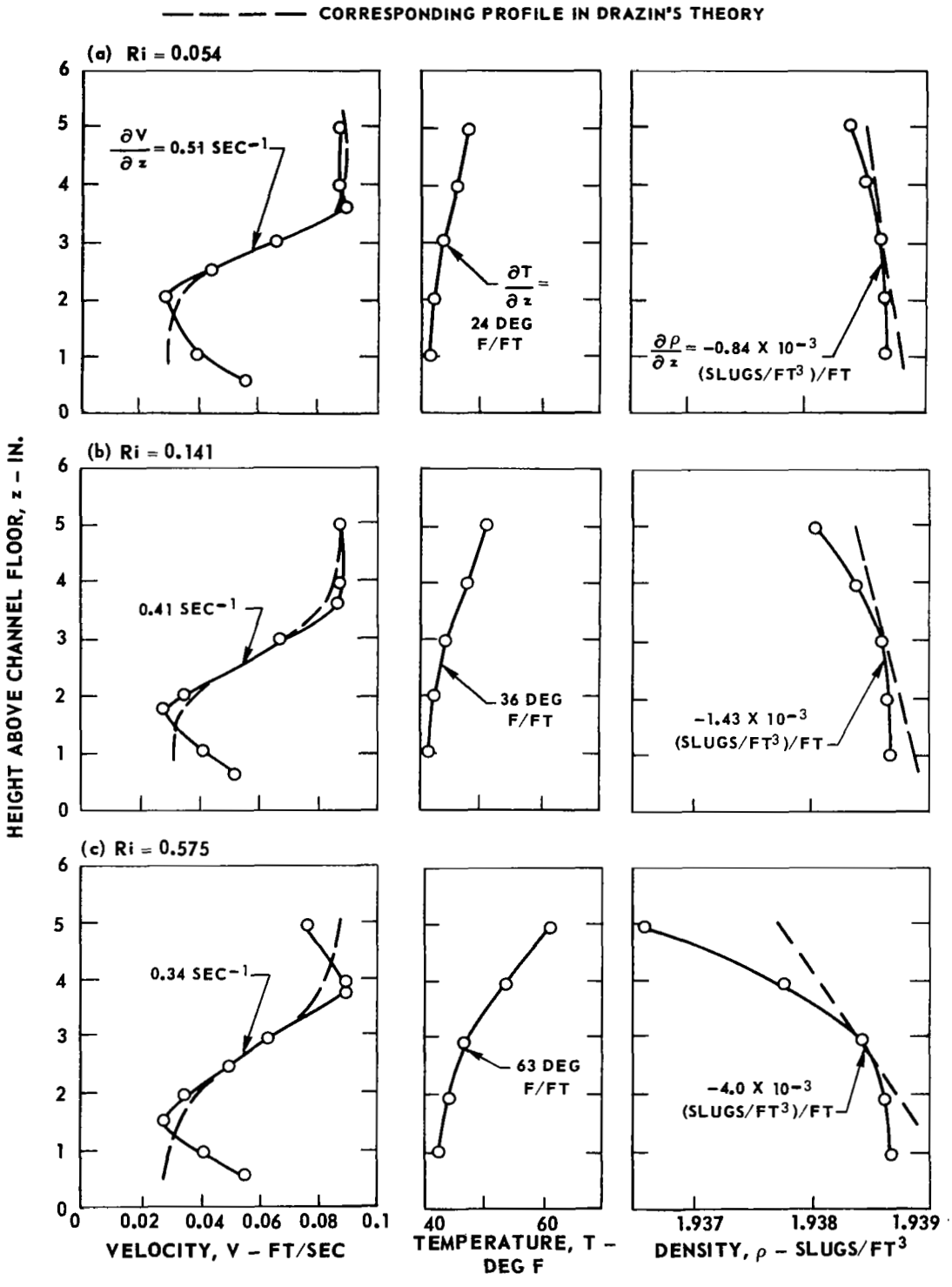

FIG. 5

TYPICAL STAGES OF BREAKDOWN OF FLOW IN SHEAR LAYER

V_O = 0.08 FT/SEC $\delta V/\delta z = -1.3$ SEC^{-1} $\delta T/\delta z = 0$

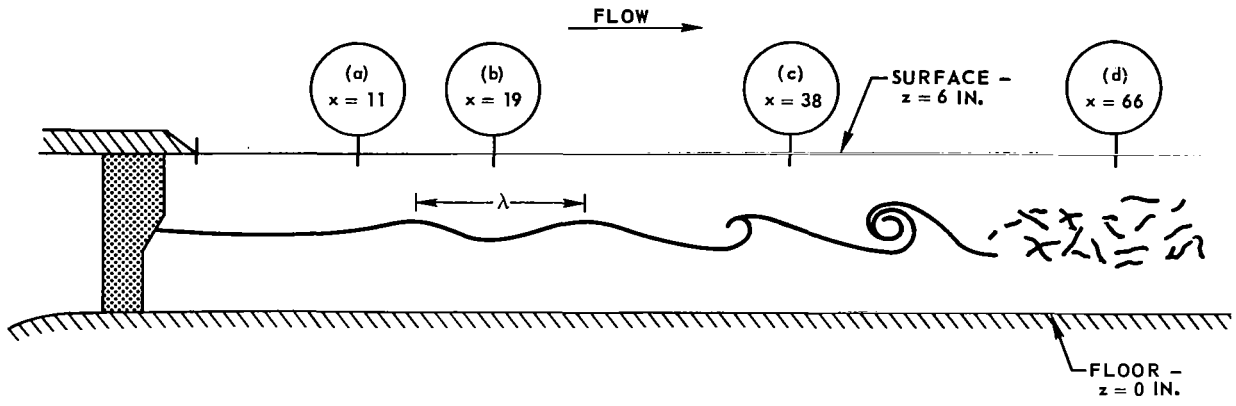

(a) x = 11 IN. – UNDISTURBED

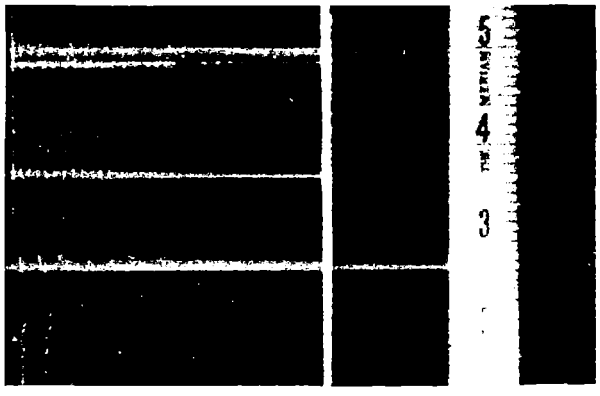

(b) x = 19 IN. – WAVES

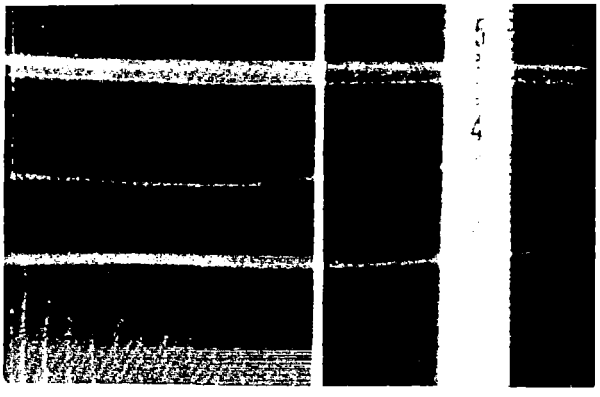

(c) x = 38 IN. – VORTICES

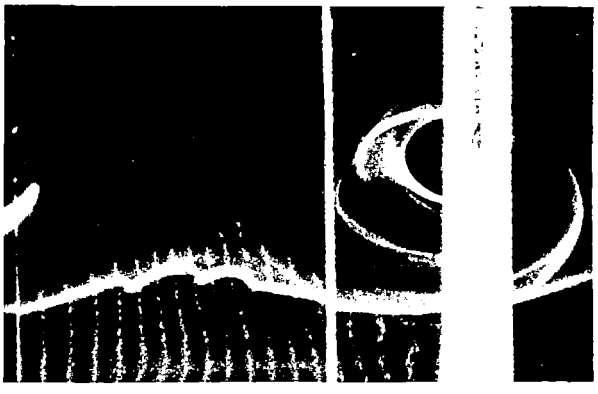

(d) x = 66 IN. – TURBULENCE

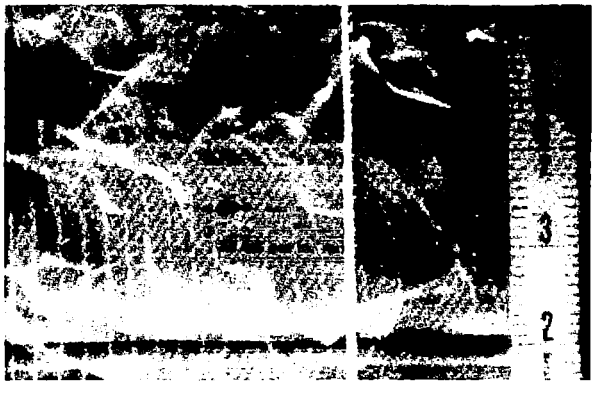

FIG. 6

ANEMOMETER TRACES FOR DIFFERENT STAGES IN BREAKDOWN OF SHEAR LAYER

$V_0 = 0.08$ FT/SEC $\quad \partial V/\partial z = -0.8$ SEC^{-1} $\quad \partial T/\partial z = 0$

SEE FIG. 5 FOR SKETCH OF FLOW PATTERN

(a) x = 10 IN. – UNDISTURBED

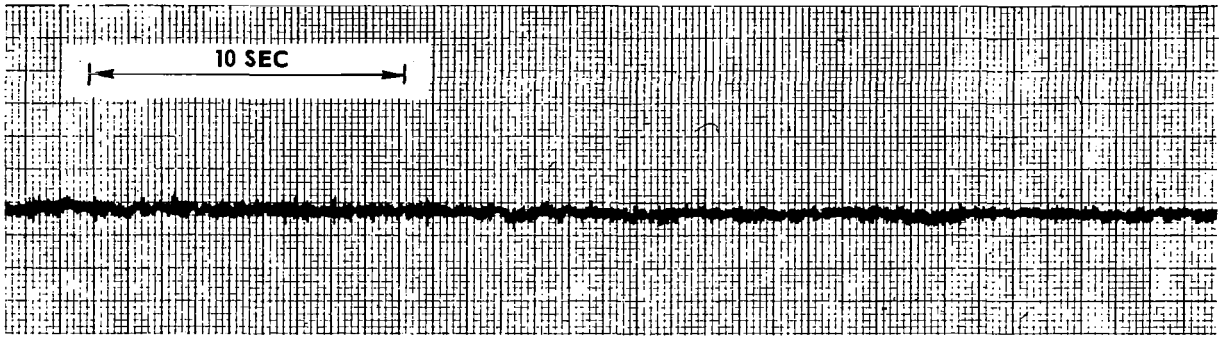

(b) x = 20 IN. – WAVES

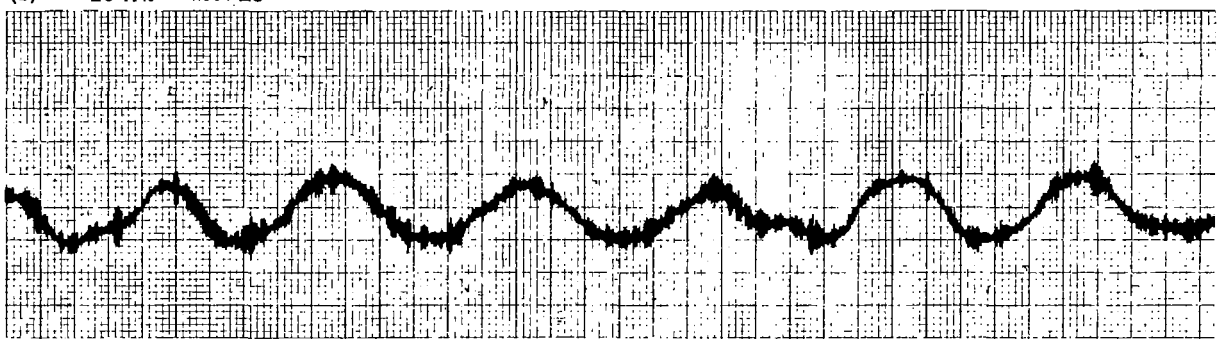

(c) x = 32 IN. – VORTICES

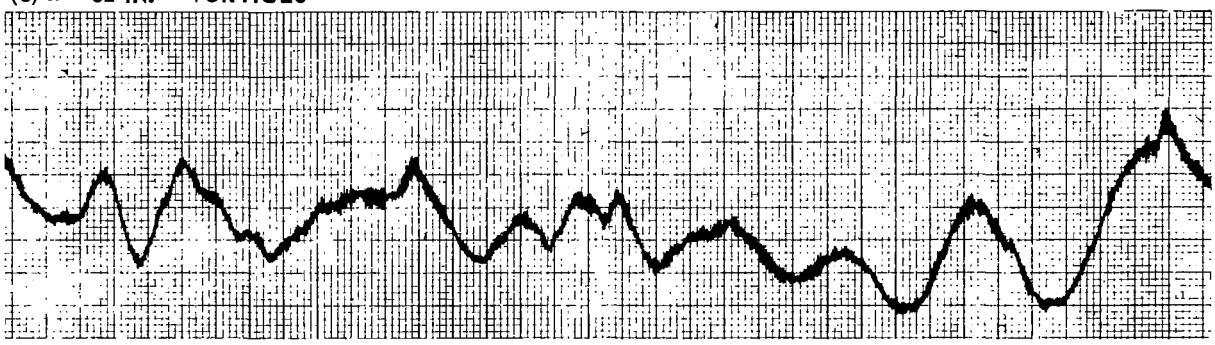

(d) x = 68 IN. – TURBULENCE

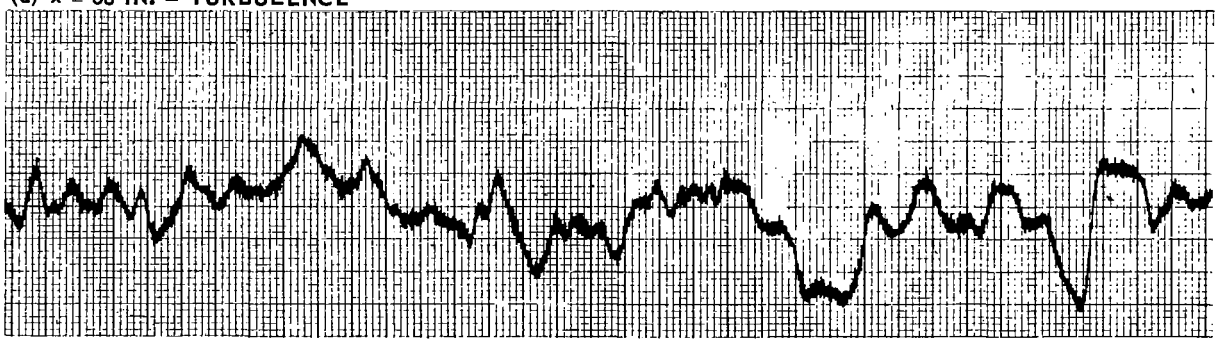

SKETCHES OF APPROXIMATE SPECTRA FOR DIFFERENT STAGES IN BREAKDOWN OF SHEAR LAYER

V_o = 0.08 FT/SEC

BASED ON ANEMOMETER TRACES IN FIG. 6

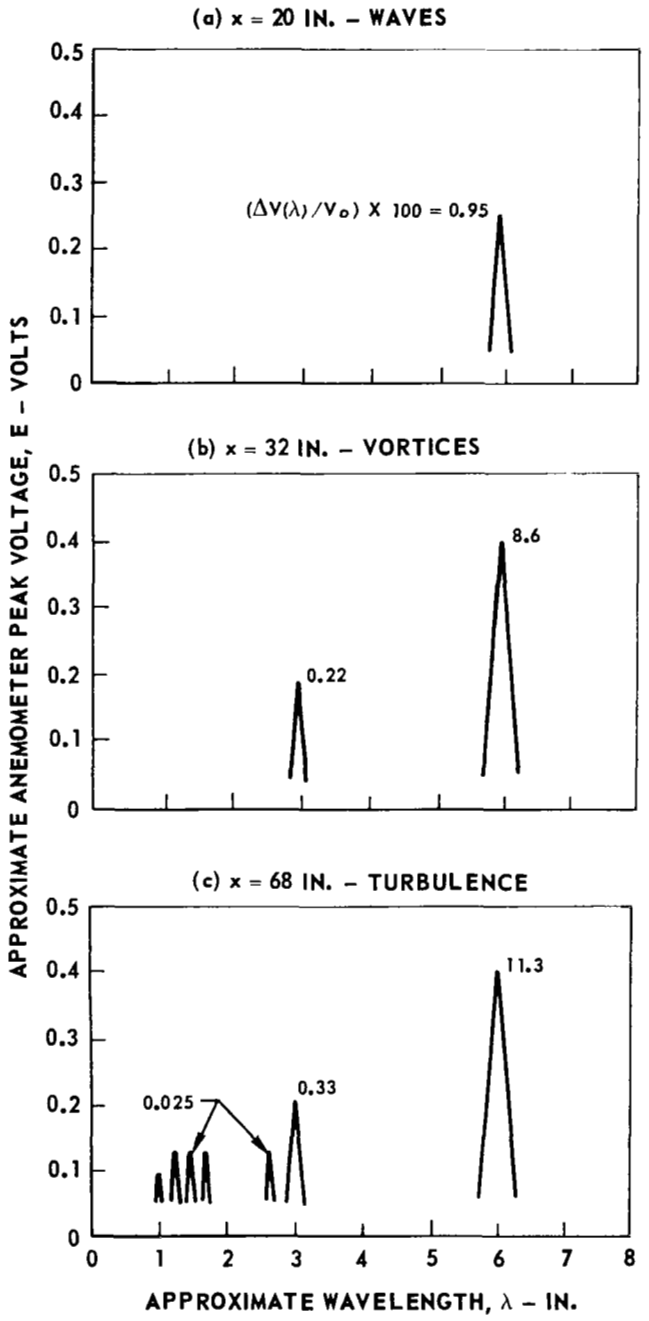

COMPARISON OF WATER CHANNEL RESULTS WITH DRAZIN'S CRITERION FOR STABILITY

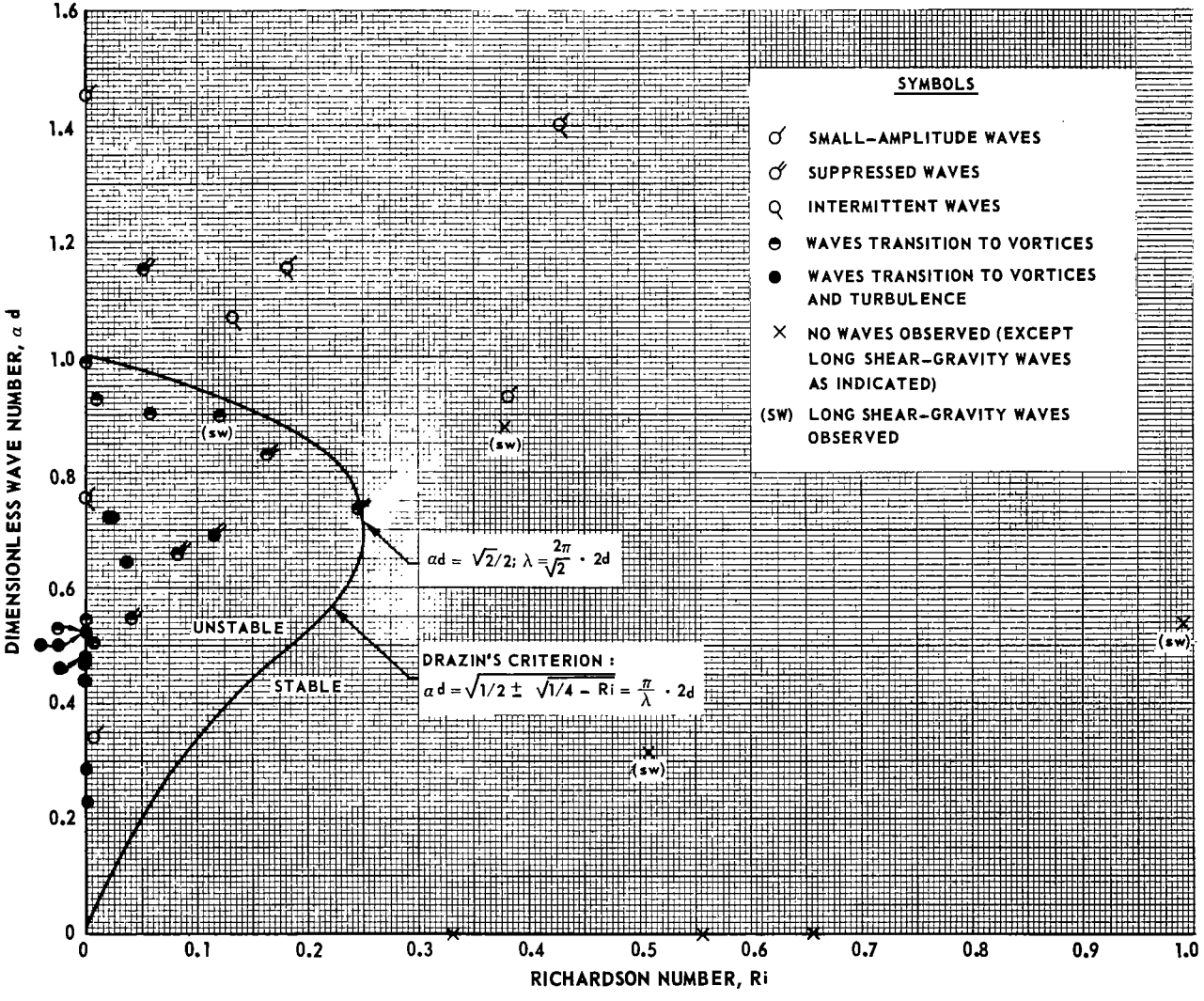

FIG. 8

EFFECT OF SHEAR ON DOWNSTREAM DISTANCE AT WHICH WAVES, VORTICES AND TURBULENCE WERE FIRST OBSERVED

SEE FIG. 5 FOR SKETCH OF TYPICAL SHEAR-LAYER BREAKDOWN
SYMBOLS SAME AS IN FIG. 8 ; $0 < Ri < 0.25$
——— ——— ———TREND IN DATA

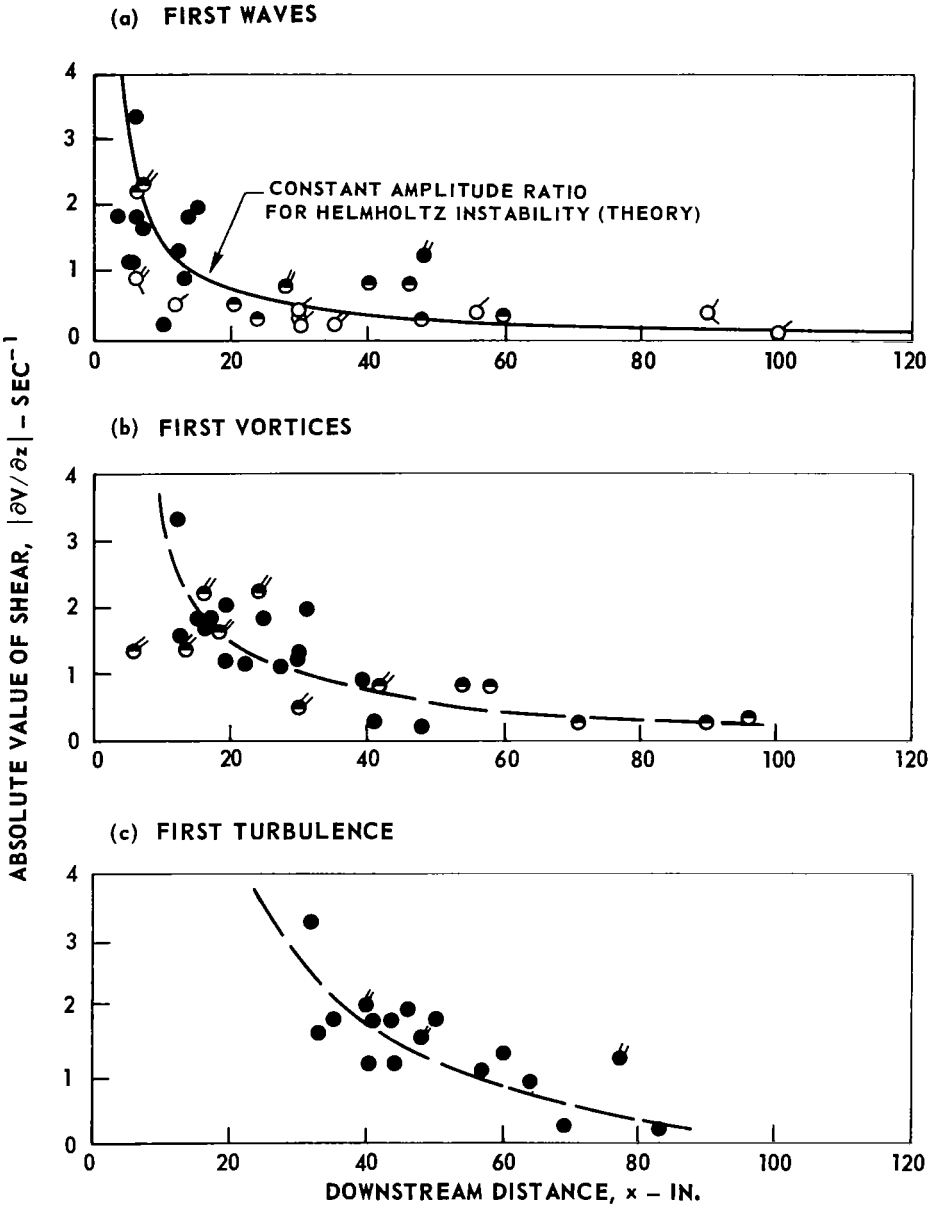

COMPARISON OF THEORETICAL STABILITY CRITERIA FOR TWO TYPES OF VELOCITY AND DENSITY PROFILES

CRITERION	VELOCITY	DENSITY
DRAZIN	$V = V_0 + \frac{\Delta V}{2}.\text{TANH}\left(\frac{z - z_0}{d}\right)$	$\rho/\rho_0 = e^{-\beta\left(\frac{z - z_0}{d}\right)}$
b = 0.2, b = 1.0 — HAZEL	$V = V_0 + \frac{\Delta V}{2}.\text{SECH}^b\left(\frac{z - z_0}{d}\right).\text{TANH}\left(\frac{z - z_0}{d}\right)$	$\rho/\rho_0 = e^{-\beta.\text{TANH}\left(\frac{z - z_0}{d}\right)}$

$$\beta = \frac{Ri \cdot d \cdot (\partial V/\partial z)_o^2}{g}$$

(a) EXAMPLES OF PROFILES

$V_0 = 0.0585$ FT/SEC, $\Delta V/2 = 0.0305$ FT/SEC, $d = 1.0$ IN.,
$z_0 = 2.7$ IN., $\rho_0 = 1.93865$ SLUGS/FT^3, $Ri = 0.14$

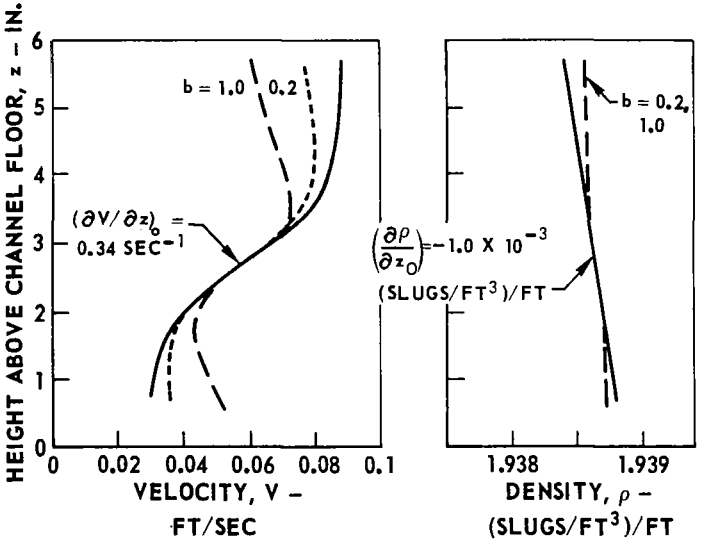

(B) CRITERIA

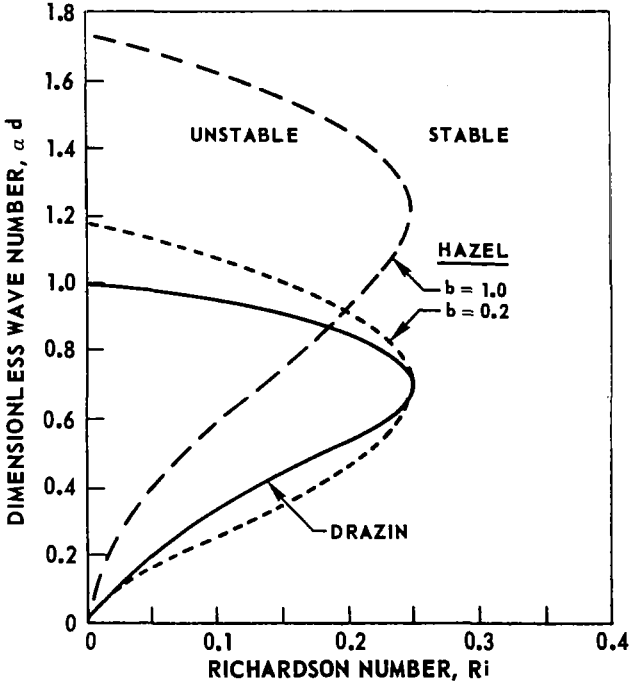

FIG. 10

EFFECTS OF LONG-WAVELENGTH WAVES ON STABILITY OF ATMOSPHERIC SHEAR LAYERS

(a) SCHEMATIC OF FLOW CONDITION

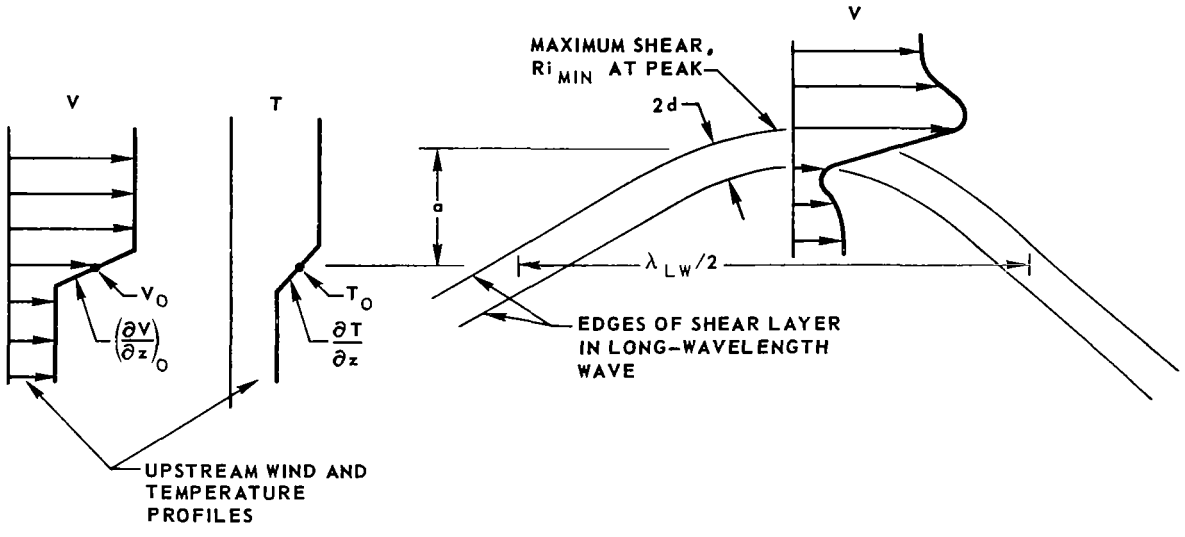

(b) EFFECT OF LAPSE RATE AND SHEAR ON Ri_{MIN} FOR TYPICAL WAVE CONDITIONS

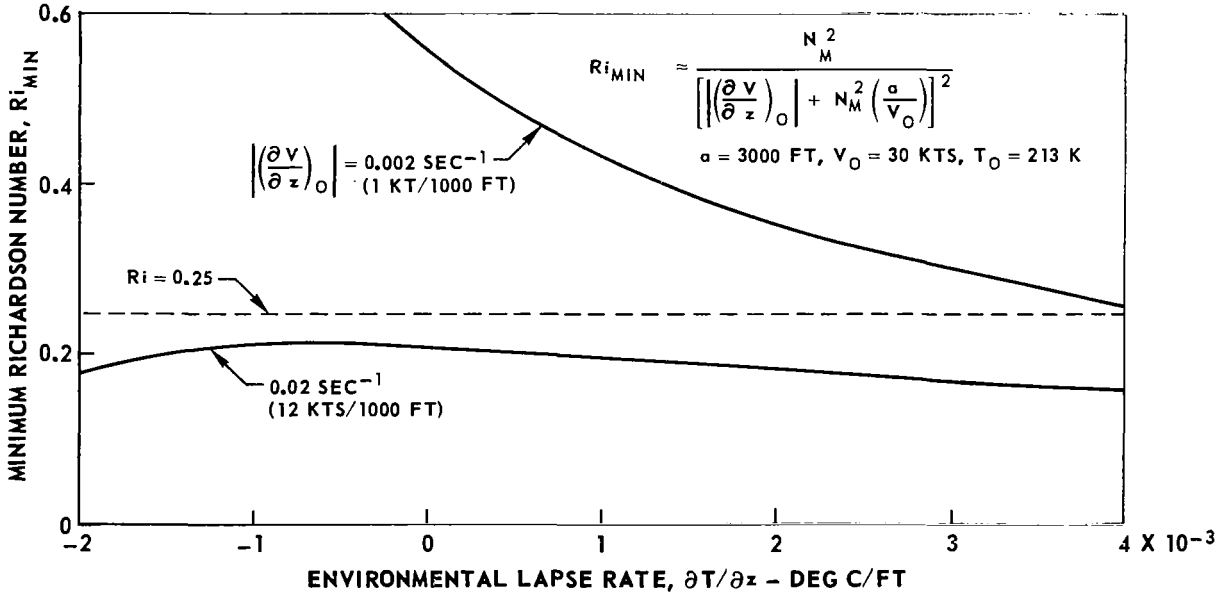

PREDICTION OF UNSTABLE WAVELENGTHS IN ATMOSPHERIC SHEAR LAYERS USING DRAZIN'S CRITERION

UNSTABLE RANGE: $\sqrt{1/2 - \sqrt{1/4 - Ri}} < \alpha d = \frac{\pi}{\lambda} \cdot 2d < \sqrt{1/2 + \sqrt{1/4 - Ri}}$

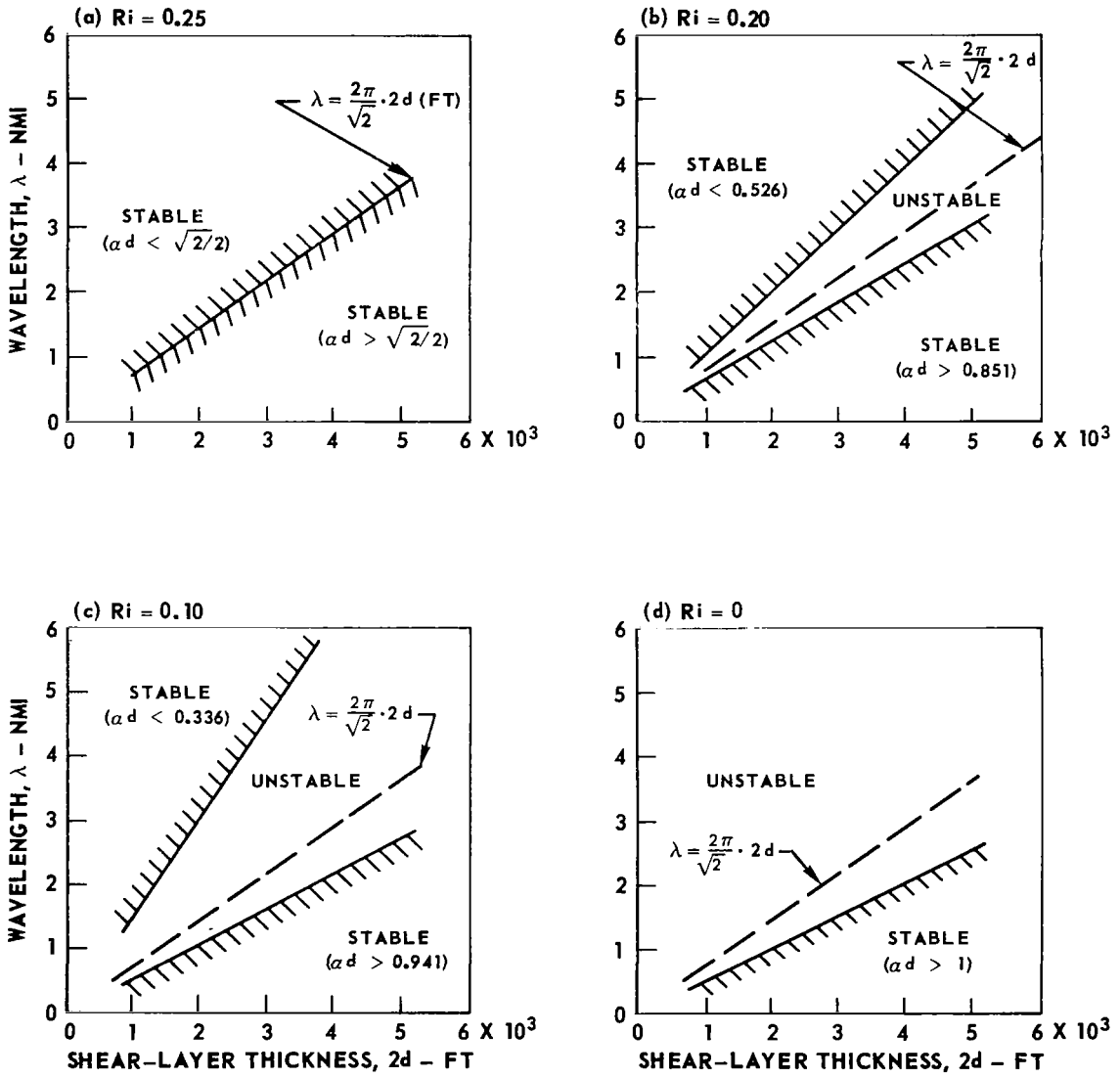

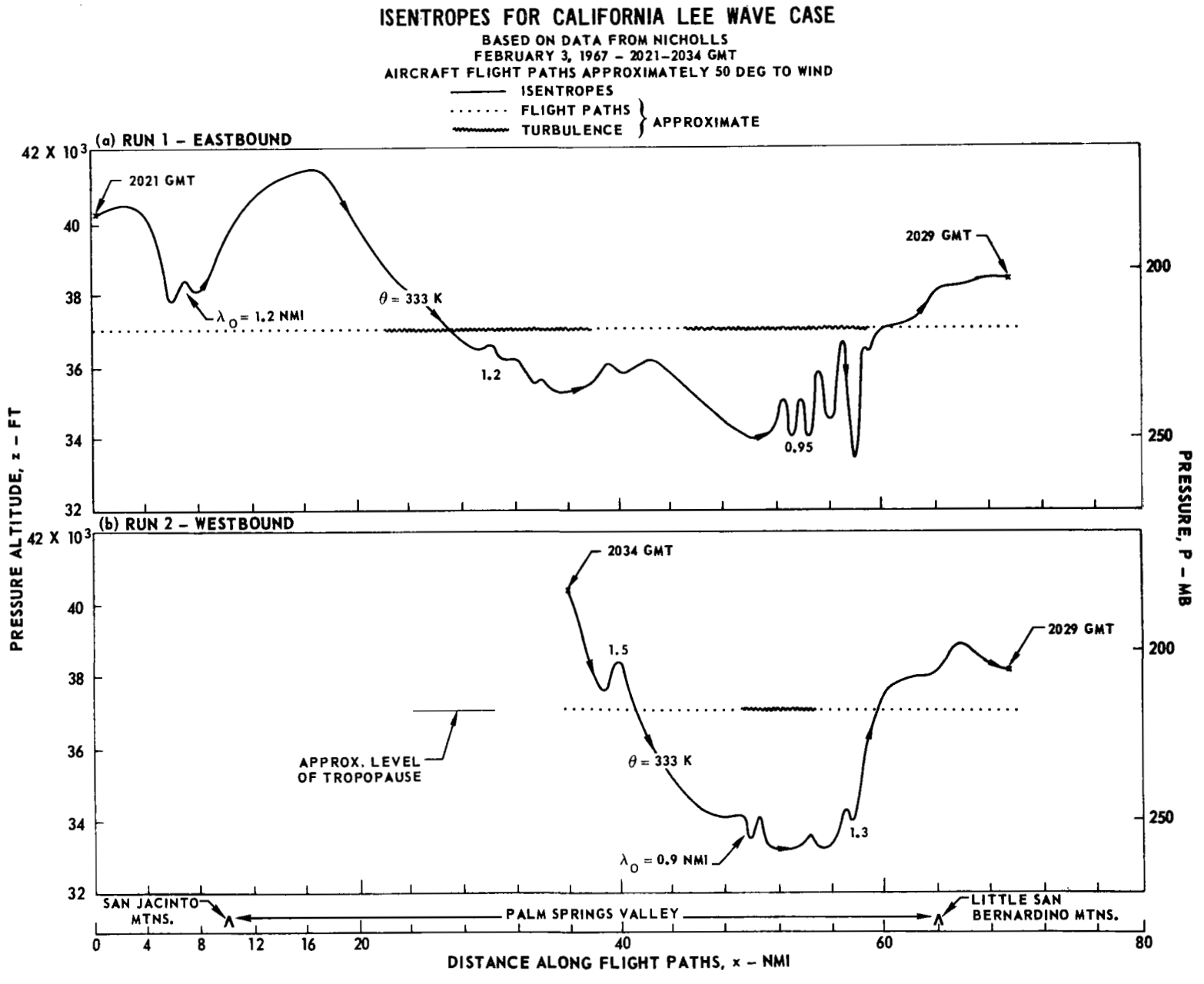
ISENTROPES FOR CALIFORNIA LEE WAVE CASE
BASED ON DATA FROM NICHOLLS
FEBRUARY 3, 1967 – 2021–2034 GMT
AIRCRAFT FLIGHT PATHS APPROXIMATELY 50 DEG TO WIND
ISENTROPES
FLIGHT PATHS
TURBULENCE
APPROXIMATE
(a) RUN 1 – EASTBOUND
2021 GMT
2029 GMT
θ = 333 K
λ0 = 1.2 NMI
1.2
0.95
(b) RUN 2 – WESTBOUND
2034 GMT
2029 GMT
1.5
θ = 333 K
APPROX. LEVEL OF TROPOPAUSE
λ0 = 0.9 NMI
1.3
42 X 10³
40
38
36
34
32
200
250
PRESSURE ALTITUDE, z – FT
PRESSURE, P – MB
SAN JACINTO MTNS.
PALM SPRINGS VALLEY
LITTLE SAN BERNARDINO MTNS.
0
4
8
12
16
20
40
60
80
DISTANCE ALONG FLIGHT PATHS, x – NMI

FIG. 13

WIND AND TEMPERATURE PROFILES FOR CALIFORNIA LEE WAVE CASE

BASED ON DATA FROM NICHOLLS
FEBRUARY 3, 1967 – 2021–2034 GMT
PROFILES ARE COMPOSITES OF AIRCRAFT AND RADIOSONDE DATA
$\lambda = (2\pi/\sqrt{2}) \times 2d$
SEE TABLE I FOR ADDITIONAL DETAILS

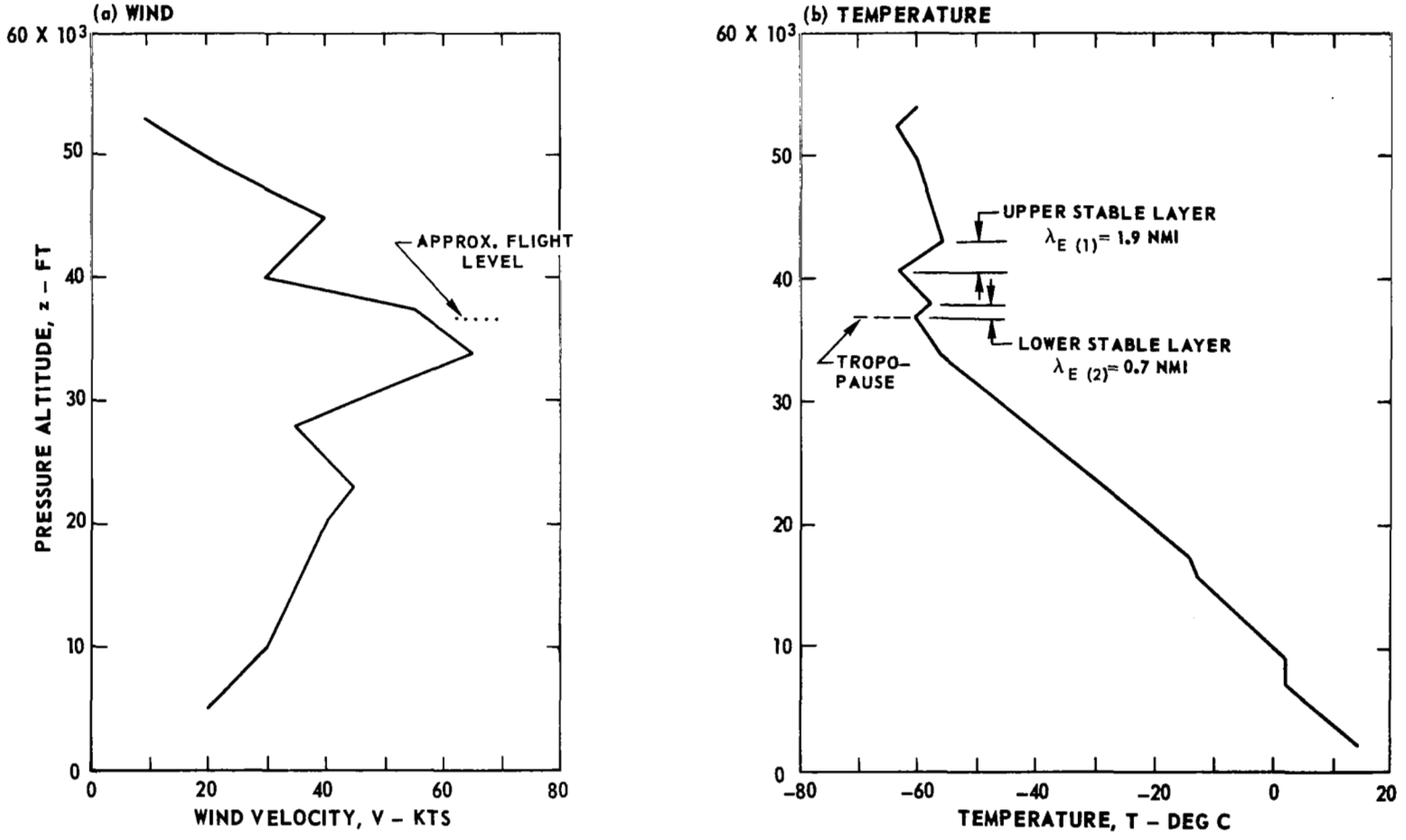

FIG. 14

ISENTROPES FOR COLORADO LEE WAVE CASE

BASED ON DATA FROM LILLY
FEBRUARY 15, 1968 – 2200–2400 GMT
AIRCRAFT FLIGHT PATHS APPROXIMATELY PARALLEL TO WIND

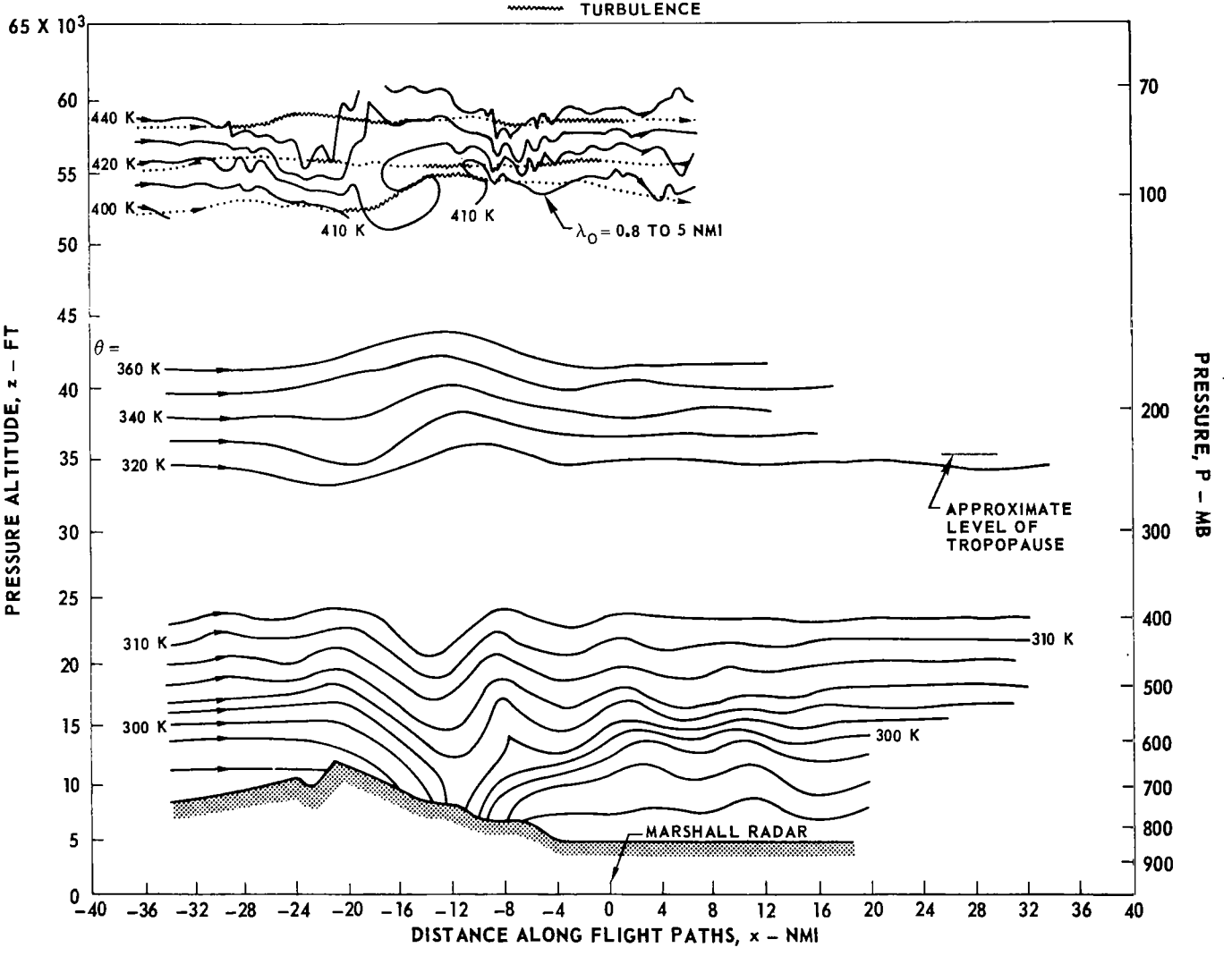

FIG. 15

WIND AND TEMPERATURE PROFILES FOR COLORADO LEE WAVE CASE

BASED ON DATA FROM LILLY
FEBRUARY 15, 1968 – 2200–2400 GMT
PROFILES FROM RADIOSONDE DATA
$\lambda_E = (2\pi/\sqrt{2}) \times 2d$
λ_E^* DENOTES WAVE UNLIKELY TO OCCUR
SEE TABLE I FOR ADDITIONAL DETAILS

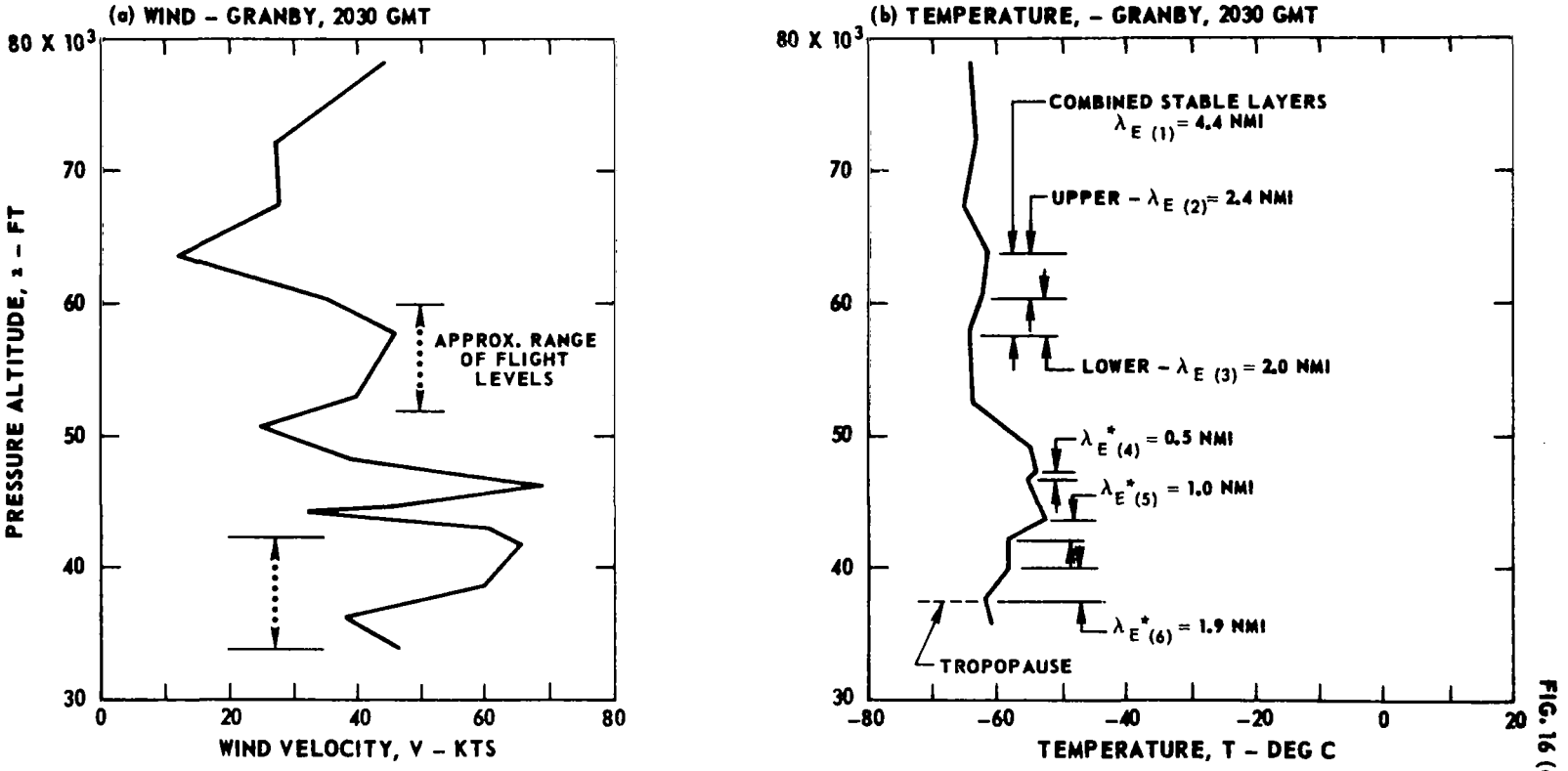

(CONTINUED)

FIG. 16 (a), (b)

WIND AND TEMPERATURE PROFILES FOR COLORADO LEE WAVE CASE

- CONTINUED -

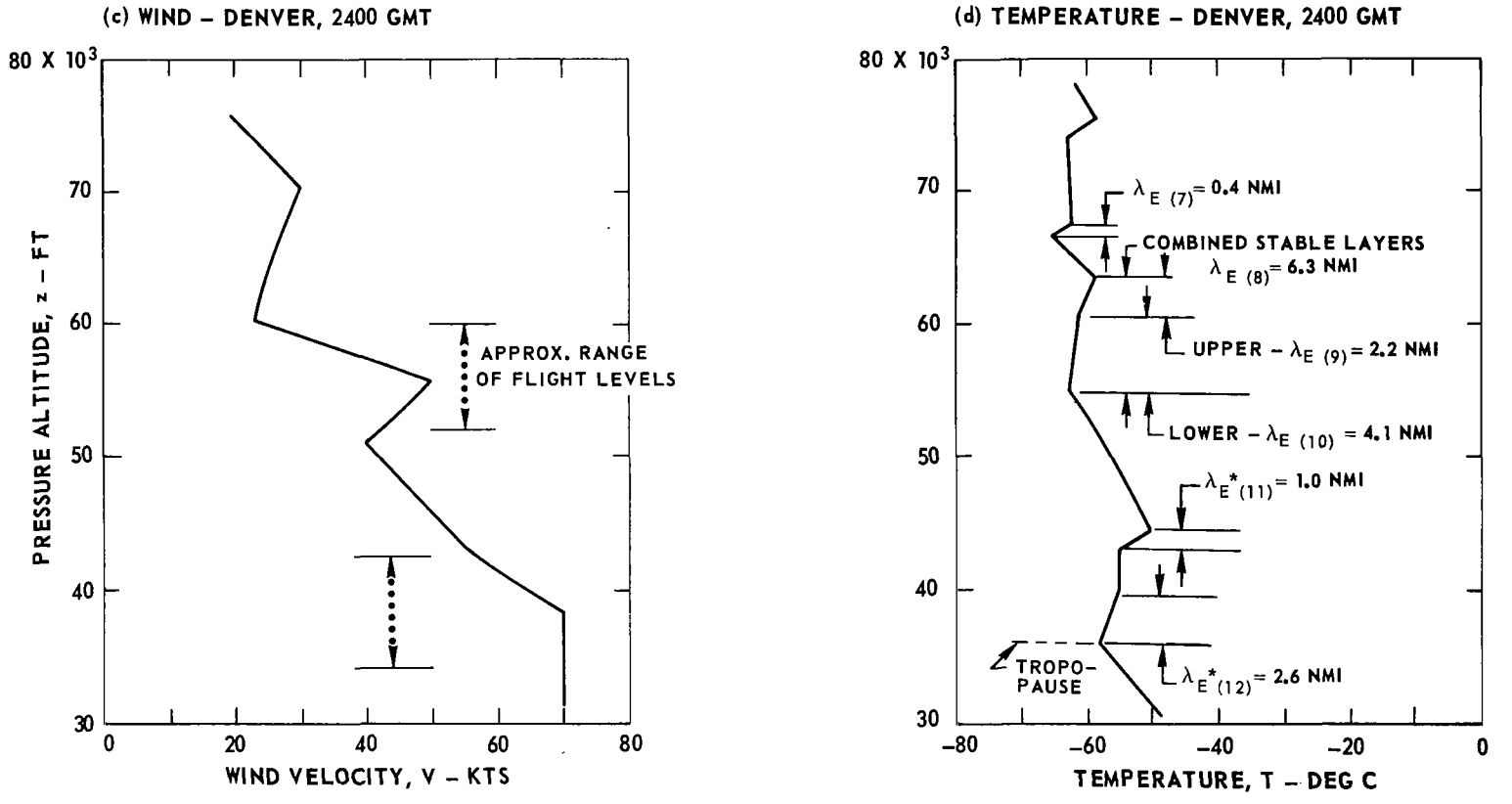

FIG. 16 (c), (d)

STABILITY BOUNDARIES FOR SHEAR LAYERS IN SHEAR–GRAVITY WAVES

$$\Delta\left(\frac{\partial V}{\partial z}\right) = \frac{2 N_M}{\eta + 1} \qquad \eta = \frac{k\epsilon}{2} \tanh(kd_1)$$

SYM	SHEAR–GRAVITY WAVE OBSERVED?
O η	YES
●	NO

*VORTICES OBSERVED; SEE TEXT

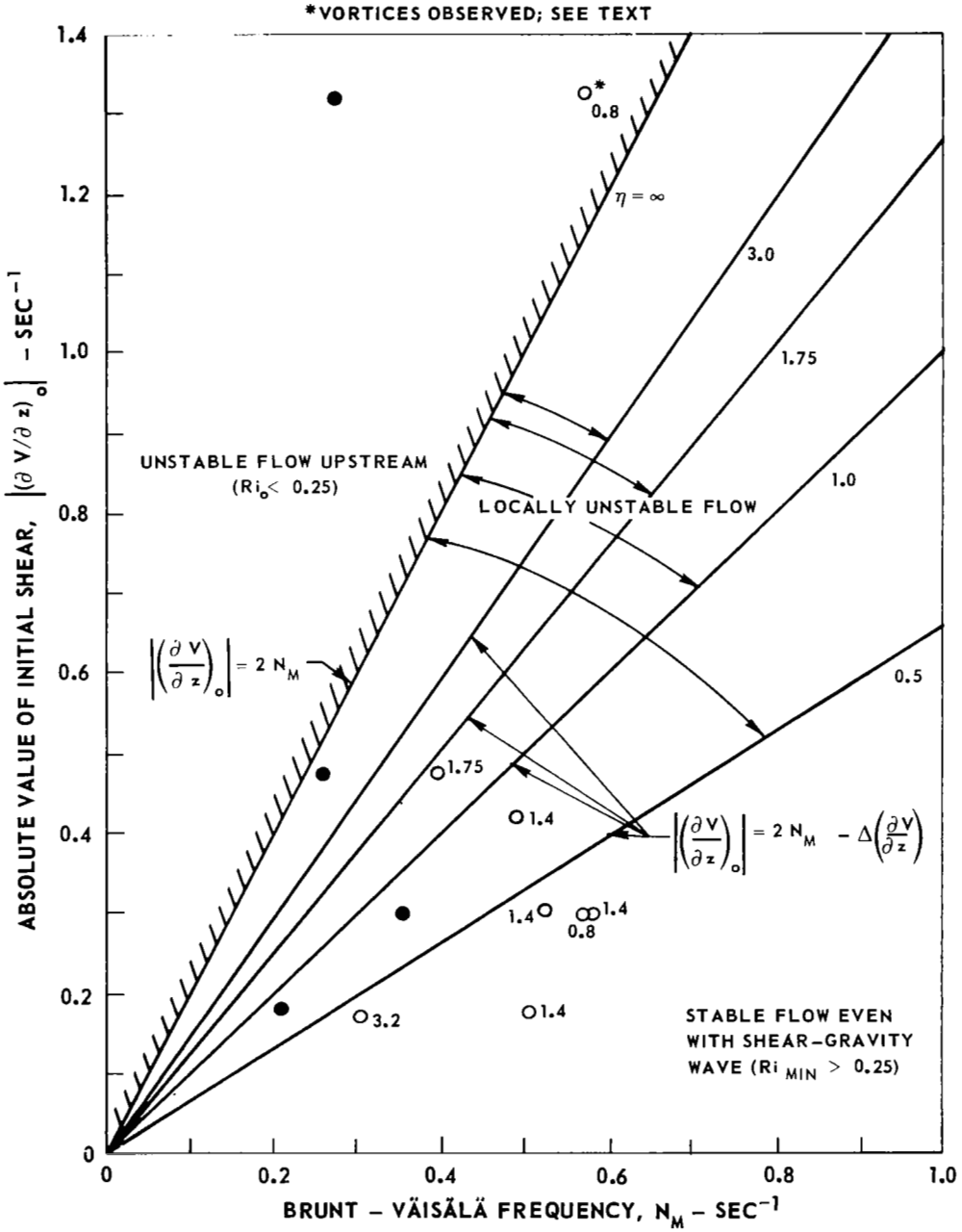

FIG. 18

PHOTOGRAPHS SHOWING INSTABILITY IN SHEAR LAYER POSSIBLY CAUSED BY SHEAR–GRAVITY WAVE

$N_M = 0.57\ SEC^{-1}$ $(\partial V/\partial z)_0 = -1.32\ SEC^{-1}$ $\eta = 0.8$

(a) UPSTREAM VELOCITY PROFILE

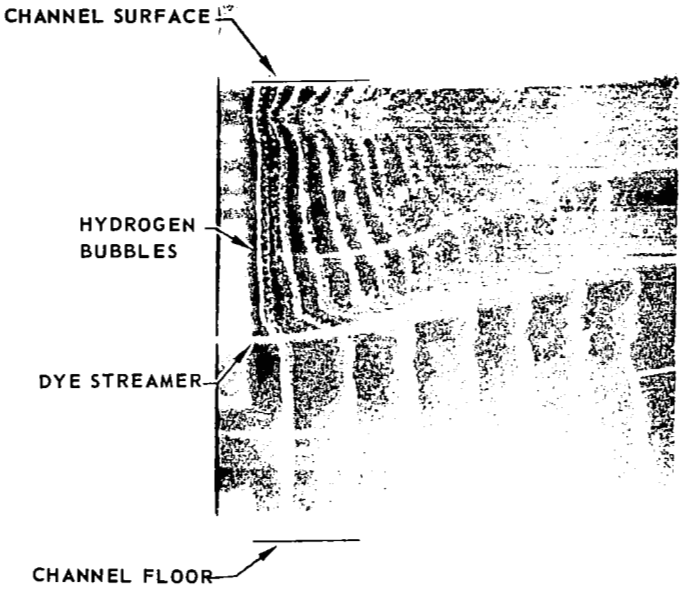

(b) VORTICES WITHIN SHEAR LAYER

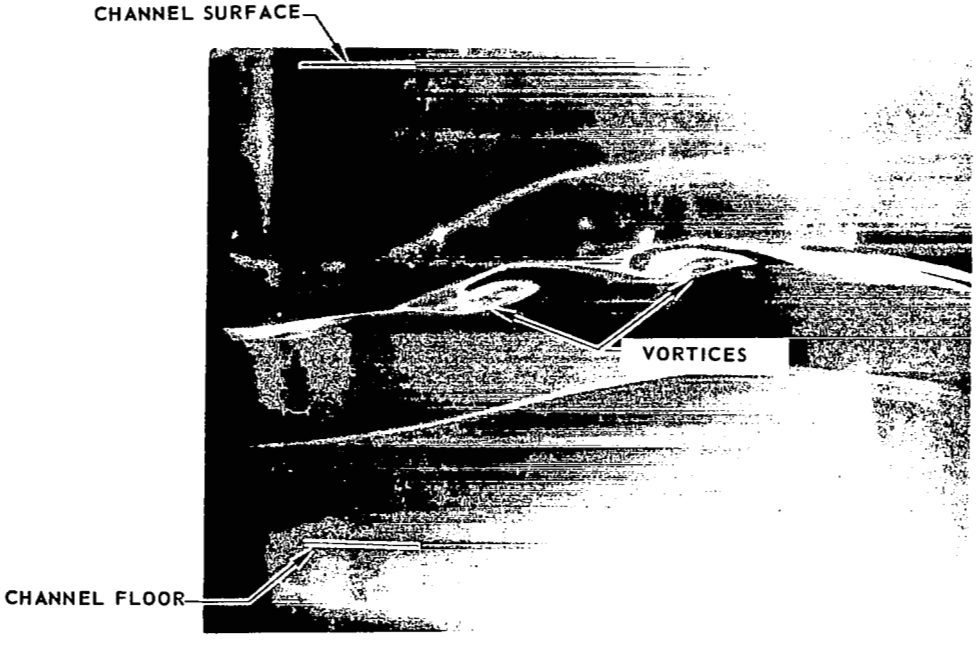

FIG. 19

EFFECT OF TRANSVERSE SHEAR ON DOWNSTREAM DISTANCE AT WHICH WAVES, VORTICES AND TURBULENCE WERE FIRST OBSERVED

CENTERLINE RADIUS = 11 FT $\partial T/\partial z$, $\partial T/\partial r$ AND $\partial V/\partial z = 0$

r/V = 100 TO 150 SEC

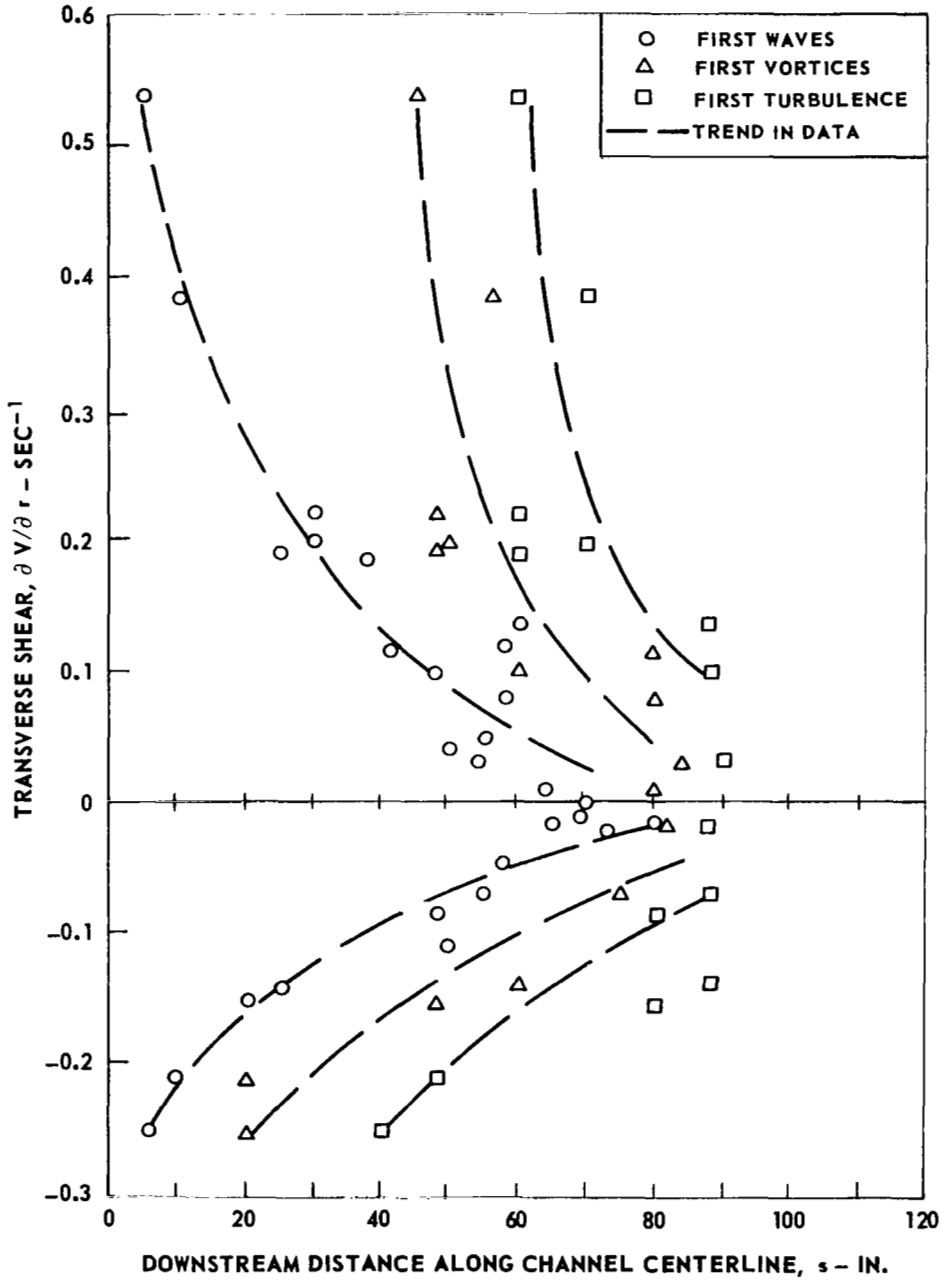

IDEALIZED CROSS SECTION SHOWING CAT ENCOUNTERS RELATIVE TO FRONTS AND TROPOPAUSE

SEE TABLE II AND APPENDIX II

CASE – 1 PROJECT JET STREAM FLIGHT 29
2 PROJECT JET STREAM FLIGHT 27
3 EAL, FLORIDA
4 UAL, WYOMING
5 WALLOPS ISLAND
6 CALIFORNIA – U-2

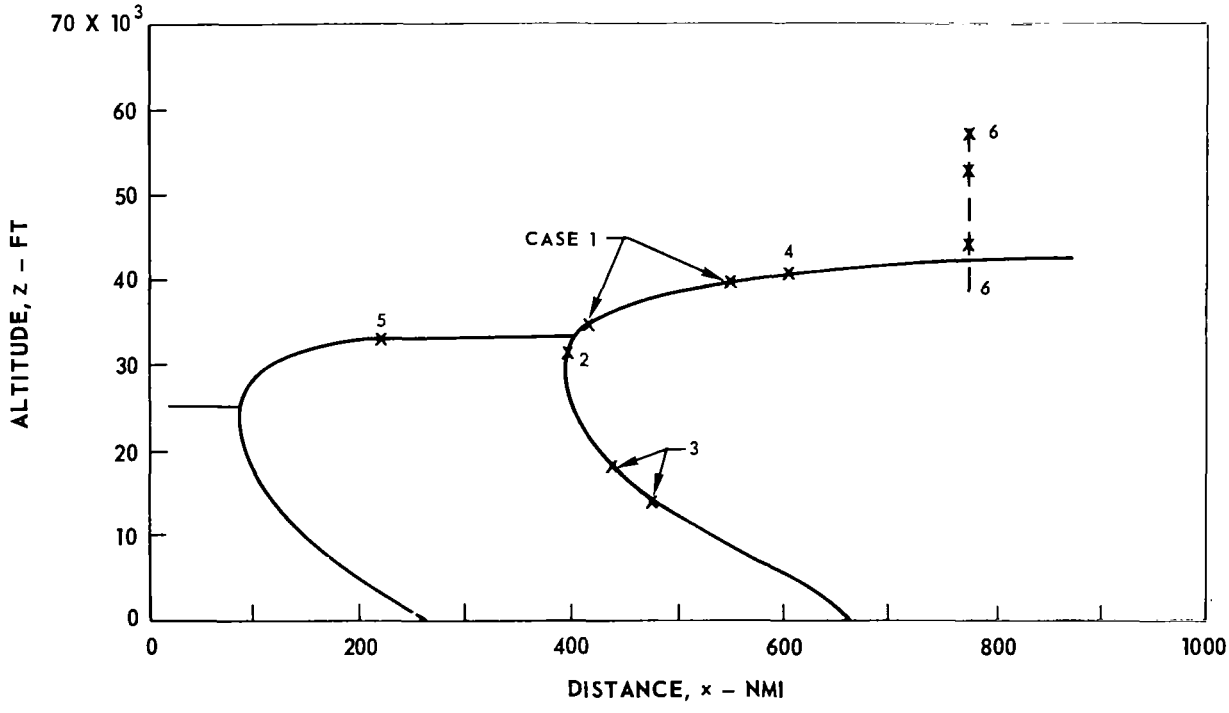

NASA-Langley, 1970 —— 20 CR-1604